

Journal of Experimental Botany, Vol. 72, No. 9 pp. 3455–3473, 2021 doi:10.1093/jxb/eraa550 Advance Access Publication 20 November 2020

This paper is available online free of all access charges (see https://academic.oup.com/jxb/pages/openaccess for further details)



RESEARCH PAPER

Abundance of metalloprotease FtsH12 modulates chloroplast development in *Arabidopsis thaliana*

Kati Mielke^{1,†}, Raik Wagner^{1,†}, Laxmi S. Mishra^{1,†}, Fatih Demir², Andreas Perrar², Pitter F. Huesgen^{2,3,4,*,} and Christiane Funk^{1,*},

- ¹ Department of Chemistry, Umeå University, 90187 Umeå, Sweden
- ² Central Institute for Engineering, Electronics and Analytics, ZEA-3, Forschungszentrum Jülich, 52425 Jülich, Germany
- ³ CECAD, Medical Faculty and University Hospital, University of Cologne, 50931 Cologne, Germany
- ⁴ Institute of Biochemistry, University of Cologne, 50674 Cologne, Germany
- [†] These authors contributed equally to this work.
- * Correspondence: p.huesgen@fz-juelich.de or christiane.funk@umu.se

Received 11 August 2020; Editorial decision 4 November 2020; Accepted 19 November 2020

Editor: Peter Bozhkov, Swedish University of Agricultural Sciences, Sweden

Abstract

The ATP-dependent metalloprotease FtsH12 (filamentation temperature sensitive protein H 12) has been suggested to participate in a heteromeric motor complex, driving protein translocation into the chloroplast. FtsH12 was immunodetected in proplastids, seedlings, leaves, and roots. Expression of Myc-tagged FtsH12 under its native promotor allowed identification of FtsHi1, 2, 4, and 5, and plastidic NAD-malate dehydrogenase, five of the six interaction partners in the suggested import motor complex. *Arabidopsis thaliana* mutant seedlings with reduced *FTSH12* abundance exhibited pale cotyledons and small, deformed chloroplasts with altered thylakoid structure. Mature plants retained these chloroplast defects, resulting in slightly variegated leaves and lower chlorophyll content. Label-free proteomics revealed strong changes in the proteome composition of *FTSH12* knock-down seedlings, reflecting impaired plastid development. The composition of the translocon on the inner chloroplast membrane (TIC) protein import complex was altered, with coordinated reduction of the FtsH12-FtsHi complex subunits and accumulation of the 1 MDa TIC complex subunits TIC56, TIC214 and TIC22-III. *FTSH12* overexpressor lines showed no obvious phenotype, but still displayed distinct differences in their proteome. N-terminome analyses further demonstrated normal proteolytic maturation of plastid-imported proteins irrespective of *FTSH12* abundance. Together, our data suggest that FtsH12 has highest impact during seedling development; its abundance alters the plastid import machinery and impairs chloroplast development.

Keywords: Arabidopsis thaliana, chloroplast, degradomics, FtsH metalloprotease, protein import, proteomics.

Introduction

Proteolysis is a degradative process that not only supplies nutrients, controls protein amounts or removes damaged or superfluous proteins, but also allows post-translational protein modifications and signaling (Turk *et al.*, 2012; Salvesen *et al.*,

2016). FtsH (filamentation temperature sensitive protein H) proteases are a family of membrane-bound metalloproteases present in eubacteria, animals, and plants. These indispensable members of the M41 peptidase family (Rawlings *et al.*,

2017) consist of an AAA (ATPase associated with various cellular activities) domain and a metalloprotease domain ligating Zn²⁺ in the consensus sequence HEXXH (where X is any uncharged residue). They are inserted into the biological membrane with one or more transmembrane helices located at the N-terminus of the enzyme (reviewed in Wagner *et al.*, 2012; Kato and Sakamoto, 2018). The AAA-type domain is involved in the formation of hexameric complexes, provides ATPase function to extract membrane substrates, and opens and closes the C-terminal hexameric cage formed by the M41 peptidase domains (Okuno and Ogura, 2013).

Compared with non-photosynthetic organisms, plants and cyanobacteria contain more FTSH genes, with 17 members present in the model plant Arabidopsis thaliana (Wagner et al., 2012). Twelve of these enzymes contain the typical zincbinding motif required for proteolytic activity, while five carry mutations in the HEXXH motif, which render them presumably proteolytically inactive; they were therefore termed FtsHi. The sub-cellular localization of eukaryotic FtsH proteins is restricted to organelles of endosymbiotic origin (mitochondria and chloroplasts). Sub-cellular fractionation in combination with immunoblot and mass spectrometric analysis identified five of the 13 plastid-localized FtsH enzymes in the thylakoid membrane, the photosynthetic membrane of the chloroplasts. Four of those FtsHs, FtsH1, 2, 5, and 8, are highly expressed and form well-studied heteromeric complexes important for the degradation and assembly of D1 protein and other transmembrane subunits of the photosynthetic machinery (reviewed in Putarjunan et al., 2013; Kato and Sakamoto, 2018). The thylakoid membrane-localized FtsH6 was recently shown to be involved in thermo-memory of seedlings of Arabidopsis (Sedaghatmehr et al., 2016), while adult plants did not show any phenotype when grown in semi-natural outdoor conditions (Wagner et al., 2011). The remaining four plastid-located FtsH proteases (FtsH7, 9, 11, and 12), as well as the five presumably proteolytically inactive FtsHi enzymes, were observed in the plastid envelope using proteomics approaches (Ferro et al., 2010). While the location of FtsH11 (Wagner et al., 2016) and FtsH12 (Li et al., 2017) in the inner envelope could be confirmed, an unexpected localization of FtsHi4 in the thylakoid membrane has been reported (Lu et al., 2014). With the exception of FTSHi3, FTSHi knock-out mutants are embryo lethal (Meinke et al., 2008), with reduced expression showing diminished Darwinian fitness (Mishra et al., 2019). A point mutation in FTSHi1 that impaired its ATPase domain function (ftsh1-1/ arc1; Kadirjan-Kalbach et al., 2012) as well as knock-down mutants of FTSHi4 (Lu et al., 2014) and FTSHi5 (Wang et al., 2018) showed cotyledon and growth phenotypes, including alterations in chloroplast ultrastructure. Plants lacking the active envelope-located protease FtsH11 were found to be sensitive to continuous light (Wagner et al., 2011) and high temperature (Chen et al., 2016; Adam et al., 2019). FtsH12 is the largest member of the presumably proteolytically active FtsH family in *A. thaliana*. *FtsH12* knock-out results in developmental arrest of the embryo (Meinke *et al.*, 2008).

Recent immunoprecipitation studies using transgenic lines overexpressing FTSH12 showed that FtsH12 forms a heteromeric 2 MDa complex with FtsHi1, FtsHi2, FtsHi4, and FtsHi5, the plastidic NAD-dependent malate dehydrogenase (pdNAD-MDH) and hypothetical chloroplast open reading frame (YCF) 2 (Schreier et al., 2018). It was further reported that this heteromeric FtsH12-FtsHi complex associates with the plastid import complex formed by the subunits 20, 56, 100, 214 (YCF1) of the translocon at the inner chloroplast envelope membrane (TIC), and drives protein import with a pulling force generated by its ATPase subunits (Kikuchi et al., 2018). Interestingly, knock-out mutants of any of the subunits of the FtsH12 motor complex are embryo-lethal, whereas single knock-out mutants of TIC20, TIC56 and TIC100 develop albino seedlings (Nakai, 2018). FtsH12 was thus suggested to be an essential component of an ATP-driven motor complex, while its proteolytic activity was reported to be dispensable (Kikuchi et al., 2013). However, neither FtsH12 orthologues nor FtsHi are found in Poaceae (Nakai, 2018; Mishra et al., 2019; Li et al., 2020), suggesting that it is not ubiquitous in all higher plants. Therefore, the importance of both the FtsH12-FtsHi complex and the interacting 1 MDa TIC complex for plastid protein import are subjects of a controversial debate (Nakai, 2015; Agne et al., 2017; Bölter and Soll, 2017; Li et al., 2020; Nakai, 2020). The consequences of modulated FtsH12 expression have not been investigated so far.

In this study, we characterized the expression and topology of FtsH12 as well as the phenotypes, morphology, proteomes, and N-terminomes of A. thaliana lines with modulated expression of FTSH12. Sub-cellular fractionation and in organello protease protection assays confirmed localization of FtsH12 in the inner envelope of the chloroplast. Diminished amounts of FtsH12 in the chloroplasts had a strong impact on the plant phenotype and plastid morphology. FTSH12 expression was not only observed in chloroplasts, but even in plastids of roots and in proplastids. Expression of Myc-tagged FtsH12 under its native promoter confirmed FtsHi1, FtsHi2, FtsHi5, and plastid NAD-MDH as interaction partners in a heterooligomeric FtsH12 complex. Seedlings with increased or reduced FtsH12 expression revealed strong changes in the proteome, including the components of the plastid protein import machinery. While the abundance of the FtsH12-FtsHi complex was diminished, TIC22-III protein accumulated in plants with reduced amounts of FtsH12. N-terminome analysis further demonstrated normal proteolytic plastid protein maturation in plants with altered FTSH12 expression. This suggests that the delayed chloroplast development in FtsH12-depleted plants was caused by limited plastid protein import capacity, which is particularly important in the early growth stages.

Materials and methods

Plant material and growth conditions

A. thaliana ecotype Columbia-0 (Col-0) was used as wild type control and as background line to generate FTSH12 miRNA knock-down mutants. A GABI-Kat T-DNA insertion line (GABI_550G09; Kleinboelting et al., 2012) was used as background line for expression of C-terminal Myctagged FtsH12 under its native promoter (Supplementary Table S1). Seeds were plated on Murashige and Skoog (MS; Murashige and Skoog, 1962) medium and when needed, supplemented with 50 µg ml⁻¹ antibiotics. After stratification at 4 °C plants were grown in short day (8 h/ 16 h photoperiod, 22 °C/18 °C, 120 µmol photons m⁻² s⁻¹). After two weeks, plants were transferred to soil and kept at short day conditions. Phenotypes of seedlings and leaves were documented using a Leica MZ9.5 microscope (Germany) or Epson Perfection 3200 PHOTOscanner (Japan). Tip-totip distance of cotyledons of two-day-old seedlings, as well as the rosette diameter of seven-week-old plants were measured using ImageI (https:// imagej.nih.gov/ij/). For etiolated seedlings, germination was stimulated by placing the seeds on plates under white light (150 μmol photons m⁻² s⁻¹) for 3-5 h, followed by growth for 5-6 d in the dark at 22 °C. The dark-grown seedlings at 0 h were harvested under low green light illumination. To identify inactive FtsHi enzymes of Arabidopsis, mutants were screened for homozygous knock-outs from a collection of heterozygous T-DNA insertion lines (Mishra et al., 2019). The T-DNA insertion lines used were as follows: FtsHi1 (AT4G23940) ARC1; FtsHi2 (AT3G16290), ftshi2-5 (SAIL 1178 A11); FtsHi4 (AT5G64580), ftshi4-1 (GK-382B06) and ftshi4-2 (SALK 067969.20.10.x); and FtsHi5 (AT3G04340), ftshi5-1 (GK-058A04).

Plasmid construction and plant transformation

Knock-down FTSH12 lines (mi12) were generated via micro-RNA constructs according to a previous report (http://wmd3.weigelworld.org/cgibin/webapp.cgi; Schwab et al., 2006). With specifically designed primers ('mi12-1/2/3 I/II/III/IV miR -s/-a/*s/*a'; Supplementary Table S1), two independent regions of FTSH12 (AT1G79560) were targeted. PCR products were cloned into the plasmid RS300 (MIR319a; Addgene, Watertown USA), cDNA from A. thaliana was generated by RevertAid RT Reverse Transcription Kit (Thermo Scientific USA). The coding sequence of FTSH12 was synthesized from cDNA with primers 'ftsh12 Forward' and 'ftsh12 Reverse for overexpressor' (Supplementary Table S1) and cloned into the binary vector pk2GW7 (VIB, Gent, Belgium) under a 35S promoter. For GUS staining, the natural promotor of FTSH12 ('ftsh12 Promotor Forward', 'ftsh12 Promoter Reverse', Supplementary Table S1) from A. thaliana gDNA was cloned into the destination vector pBGGUS (Kubo et al., 2005) by fusing it with the GUS reporter gene. A fusion construct was synthesized by overlapping PCR using the amplified FTSH12 promoter and CDS as template and the primers 'ftsh12 Promoter Forward' and 'ftsh12 Reverse for cmyc-line' (Supplementary Table S1). The pftsh12::ftsh12CDS was cloned into a pENTR/D-TOPO vector and transferred into the destination vector pGWB16 resulting in a gene product with 4× c-myc tag. Binary plasmids were transformed into electro-competent Agrobacterium tumefaciens [GV3101::pMP90 (pTiC58DT-DNA); Hellens et al., 2000]. Non-segregating T2 lines of A. thaliana Col-0 were transformed as described by Clough and Bent (1998). Heterozygous T-DNA insertion lines of the GABI-KAT collection (Kleinboelting et al., 2012) were transformed with the T-DNA inserted into FTSH12 (GABI_550G09). Presence of the c-myc-fused gene product in the T2 generation was confirmed immunologically using anti-FtsH12 antibodies.

Arabidopsis cell culture

The A. thaliana Col-0 cell culture was grown in MS medium supplied with 3% (w/v) sucrose (pH 5.7) at 25 °C in darkness (Pesquet et al., 2010; Dubreuil et al., 2018). Cells were sub-cultured weekly by 1:10 dilution. To immunodetect FtsH12, seven-day-old cells grown in darkness were sub-cultured (1:10 ratio) in MS medium supplied with 1% sucrose and placed in continuous light (150 µmol photons m⁻² s⁻¹). Sampling took place after 0, 1, 5, 7, and 14 d of illumination. Cells were pelleted without centrifugation and snap frozen in liquid nitrogen.

Histochemical staining of β-glucuronidase (GUS)

Seedlings, leaves, and roots were fixed in 90% acetone at −20 °C for 60 min. Siliques were sliced open before fixation. GUS staining was performed as described by Vielle-Calzada et al. (2000). Samples were visualized using a Leica MZ9.5 or Axioplan 2 imaging microscope (Carl Zeiss, Germany).

Histochemical detection of reactive oxygen species (ROS)

ROS staining was carried out as described by Fryer et al. (2002). The experiments were performed on 10-day-old seedlings grown in continuous light for 7 d. ROS staining of plants grown in short day conditions was included as control. To visualize superoxide (O2:-), the nitroblue tetrazolium (NBT) staining method was used. Hydrogen peroxide (H2O2)staining was carried out by using 3,3'-diaminobenzidine (DAB).

Determination of chlorophyll and anthocyanin content

Chlorophyll extraction was performed on 10-week-old plants grown under short day conditions by grinding the leaves (100 mg) in buffered acetone solution, as described by Porra et al. (1989). Anthocyanin extraction was performed on etiolated seedlings harvested at 0 h, day 1, and day 2, as described by Nakata et al. (2013).

Determination of chlorophyll fluorescence parameters

Pulse-Amplitude Modulation (PAM) was measured on seven-week-old plants kept in continuous light for 7 d; plants grown in short day conditions were included as control. All plants were dark adapted for at least 30 min prior to measurements. A PAM-210 fluorimeter (Walz, Germany) was used for measurements over time, with increasing photosynthetic active radiation.

Chloroplast isolation and sub-fractionation

Chloroplast isolation and sub-fractionation was performed as described by Wagner et al. (2016).

Protease protection assay

A. thaliana plants were grown in a light/ dark cycle of 8 h/ 16 h. Chloroplasts were isolated according to Sun et al. (2011). The protease protection assay was carried out as described by Knopf et al. (2012).

Protein extraction

Total protein was extracted from 10 day-old seedlings in extraction buffer [50 mM Tris-HCl, pH 7.5, 5 mM EDTA, 10% (v/v) glycerol, 0.5% (w/v) lithium dodecyl sulfate (LDS), 10 mM DTT and protease inhibitor (one tablet per 10 ml buffer; Pierce Thermo Scientific USA) in a mortar precooled with liquid nitrogen. The protein content was quantified using the RC DC Protein Assay Kit (Bio-Rad USA).

SDS-PAGE and immunoblotting

A total of 15 µg protein per sample was separated on a TGX GEL 4-20 % (Bio-Rad), according to the method described by Laemmli (1970),

3458 | Mielke *et al.*

and transferred to polyvinylidine difluoride (PVDF) membranes (Bio-Rad), as described by Towbin *et al.* (1979). Antigen–antibody complexes were visualized using WesternBright Quantum HRP substrate (Advansta, USA) and the Bio-Rad ChemiDocTM Imaging Systems (UK).

Immunoblotting was performed as described by Wagner *et al.* (2016). A polyclonal antibody directed against the C-terminal FtsH12 peptide sequence DRVSYQPVDLRAAPLHRS was raised in rabbit and was produced at Agrisera, Sweden. Antibodies against CP43 and TOC75 were purchased from Agrisera AB (Sweden; see Wagner *et al.*, 2016).

Determination of chloroplast size

Cotyledons of two-day-old seedlings were sliced in isotonic buffer [20 mM Tricine pH 7.8, 0.33 M sorbitol, 5 mM EDTA, 10 mM Na₂CO₃, 0.1% (w/v) BSA]. Released chloroplasts were visualized with an Axioplan 2 light microscope (Carl Zeiss, Germany). The open source image processing program ImageJ (Java-based image processing program developed at the NIH) was used for measuring chloroplast length and width. Average diameters were calculated by dividing the sum of length and width by 2.

Transmission electron microscopy (TEM)

Transmission electron microscopy was used to study chloroplast morphology in cotyledons of 10-day-old seedlings, and in true leaves of nine-week-old plants of wild type and two FTSH12 knock-down lines (mi12-2 and mi12-3). In the FTSH12 knock-down lines, only the morphology of chloroplasts in variegated leaf areas was analyzed. Leaf samples were fixed with 2.5% glutaraldehyde in 0.1 M sodium cacodylate buffer, while the cell suspension was post-fixed in 1% osmium tetroxide, dehydrated with ethanol, propylene oxide and finally embedded in Spurr resin, according to standard procedures (Wagner et al., 2016). Chloroplast length and width were measured by using ImageJ software; average diameters were calculated by dividing the sum of length and width by 2.

RNA extraction and gRT-PCR

RNA extraction and quantitative real-time polymerase chain reaction (qRT-PCR) was performed as described by Mishra et al. (2019).

Seedling proteome and terminome analysis

Four replicates of seeds from wild type, miRNA mi12-3, and oxp12-1 were grown on MS media plates for two days, with 24 h difference between each replicate sowing. Seedlings were harvested and homogenized in 100 mM HEPES, 5 mM EDTA, 4 M guanidinium chloride (GuHCl), pH 7.5, with 1x Halt protease inhibitors (Thermo Fisher, Germany) using a mortar and pestle. Homogenates were filtered through a 100 μm nylon mesh, centrifuged at 500 × g for 1 min at 4 °C, and the filtrate was centrifuged at 10 000 \times g for $\bar{1}$ min at 4 °C. Proteins in the supernatant were purified by chloroform/methanol precipitation (Wessel and Flügge, 1984) and resolubilized in 6 M GuHCl, 100 mM HEPES pH 7.5. Protein concentration was estimated using the BCA assay (Bio-Rad). For each replicate of each genotype, 100 µg proteome was used for label-free quantitative proteome analysis, and 1 mg proteome for N-terminome analysis. An estimated 100 µg protein of each sample was reduced with 5 mM dithiothreitol for 30 min at 56 °C, cooled to 20 °C and alkylated with 15 mM iodoacetamide for 30 min in darkness, before 1:6 dilution with water, addition of 5 mM CaCl2 and 5% (v/v) acetonitrile (ACN). The samples were digested with 1 µg MS-grade approved trypsin (SERVA, Germany) overnight at 37 °C, before addition of a further 0.5 µg trypsin and incubation for 2 h at 37 °C. For terminome analysis, 1 mg wild type, mi12-3 and ox12-1 seedlings, proteomes were differentially labeled with stable isotope at the N-terminus and Lys side chain primary amines, using ¹²CH₂O and sodium cyanoborohydride (for wild type), ¹²CD₂O and sodium cyanoborohydride (for *mi12-3*), and ¹³CD₂O and sodium cyanoborodeuteride (for *ox12-1*), as described previously (Demir *et al.*, 2017). Proteins were digested with trypsin and N-termini enriched with a development version of the HUNTER protocol (Weng *et al.*, 2019). Briefly, free trypsin-generated primary amines of internal and C-terminal peptides were modified by hydrophobic tagging with undecanal, the solvent was removed, the pellet resuspended and applied on to a reverse phase solid phase extraction cartridge (SepPak C18, Waters, UK). Dimethylated or endogenously blocked N-terminal peptides were eluted with a stepped gradient from 15–50% (v/v) ACN, whereas hydrophobically tagged, trypsin-generated peptides remained bound to the cartridge under these conditions (Chen *et al.*, 2016).

Co-immunoprecipitation (Co-IP) of FtsH12-4×c-myc

Chloroplasts of six-week-old *pftsh12::ftsh12CDS::4×c-myc* in GABI_550G09 background were isolated as described above. Plastids were solubilized in PBS, 0.28% beta-DM and 1.86% digitonin. Immunoaffinity enrichment of c-myc tagged FtsH12 and mass spectrometry-based identification of co-precipitating proteins was performed according to Haselmann *et al.* (2018). Antibodies used were monoclonal mouse antic-myc and mouse anti-His (Thermo Fisher Scientific). Briefly, proteins eluted after affinity capture were purified with SDS-PAGE and in-gel digested with trypsin (SERVA), as described earlier for proteome analysis by mass spectrometry.

Mass spectrometry data acquisition

Peptides were de-salted using C18 STAGE-tips (Rappsilber et al., 2007) before analysis with an Ultimate 3000 RSLCnano chromatography system (Thermo, Germany) operated in a two-column setup (Acclaim PepMap100 2 cm trap, 25 cm or 50 cm analytical column). The nanoLC system was linked online to an Impact II high resolution Q-TOF mass spectrometer (Bruker, Germany) via a CaptiveSpray nano ESI source (Bruker), essentially as described previously (Beck et al., 2015). For shotgun proteome analysis, an estimated 1 µg of desalted peptides was loaded, for terminome experiments 50% of each fraction, and for AP-MS experiments, 50% of the sample was loaded.

Mass spectrometry data analysis

Peptides were identified and quantified using MaxQuant v 1.6.0.16 (Tyanova et al., 2016a). The UniProt Arabidopsis protein database (downloaded on 01/2018, 41 350 entries) was used for spectrum-to-sequence matching. For the label free quantitative (LFQ) proteome data, search parameters included trypsin digest enzyme, allowing for up to two missed cleavages, Cys carbamidomethylation as fixed, and N-terminal acetylation and Met oxidation as variable modification. False discovery thresholds of 0.01 were applied at the level of peptide-spectrum matching (PSM) and for protein identifications, two quantification events were required for quantification, and the "match between runs" option in MaxQuant was enabled for replicates within each group/genotype. The "calculate iBAQ values" option was enabled. Further analysis was performed using the Perseus statistical software package v1.6.1.1 (Tyanova et al., 2016b). Contaminants, reverse hits, and proteins identified only by modified peptides were excluded. Results were filtered for protein groups quantified in at least two out of four biological replicates in at least one genotype, LFQ intensities were log₂-transformed, and missing values imputed using Perseus standard settings. Significant differences in protein accumulation were determined by ANOVA analysis with Benjamini-Hochberg false discover rate (FDR)<0.05, followed by Tukey's honest significance test. Differentially regulated proteins were also clustered and analyzed for functional KEGG term enrichment and protein interactions using STRING db v.11, using a high confidence database, experimental

and co-expression information only (Szklarczyk et al., 2018). For N-terminome analysis, MaxQuant search parameters were adapted to semi-specific (free N-terminus) ArgC as digestion enzyme, isotope labeling by light (+28.031300) and/or heavy (+36.075670) dimethylation of Lys residues and peptide N termini, Cys carbamidomethylation as fixed and Met oxidation, N-terminal acetylation (+42.010565) or N-terminal pyroGlu formation from Glu (-18.010565) or Gln (-17.026549) as variable modifications (Hofsetz et al., 2020). Identified N-termini were annotated based on the modification of SpecificPeptides.txt file of the MaxQuant output folder, with information from Uniprot.org, using an in-house script (MaxQuant Advanced N Termini Interpreter, MANTI. pl version 3.9.5, https://sourceforge.net/projects/manti/). The prediction of sub-cellular localization and signal peptide (SP) or transit peptide (TP) cleavage sites was retrieved from TargetP2.0 (Almagro Armenteros et al., 2019). Protein termini were considered significantly changed in abundance between two genotypes if they passed a Linear Model for Microarray Analysis (LIMMA)-moderated t-test (Ritchie et al., 2006; Gomez-Auli et al., 2016) with P<0.05, and changed more than 50% in abundance (log₂>0.58 or <-0.58).

Results

FtsH12 is expressed in non-photosynthetic plastids, located in the inner envelope with its C-terminus exposed to the stroma

While most active FtsH proteases in Arabidopsis thaliana arose after an evolutionary recent gene duplication event Wagner et al., 2012, FtsH12 is not part of a homologous pair. This protease has a higher molecular weight (112 kDa) than the other active FtsH enzymes due to a longer N-terminal stretch (Supplementary Fig. S1A) containing two transmembrane helices (Supplementary Fig. S1B). Furthermore, three conserved amino acids in the Walker B motifs are exchanged (F587 for I) and second region of homology (SRH) (E651 for A and F652 for L), compared with the consensus sequence that might impair ATP hydrolysis (Supplementary Fig. S1C). In the catalytic HEXXH motif, described as "abXHEbbHbc", the "a" in active metalloproteases is most often a valine or threonine, "b" an uncharged residue, and "c" a hydrophobic residue. In FtsH12, however, an unusual leucine is placed at the "a" site, according to Interproscan (Supplementary Fig. S1C). Arabidopsis eFP browser (data accessible at http://bar. utoronto.ca) indicates stronger expression of FTSH12 and other subunits of the FtsH12/FtsHi complex in photosynthetic tissues, but also marked expression in roots, flowers and seeds (Supplementary Fig. S2A; for comparison, expression of the thylakoid-located FtsH2 and of the import complex subunit YCF1 are shown). GUS staining in FTSH12 promoter fusion lines confirmed expression of FTSH12 in young vegetative plant leaves and roots, as well as in generative organs and embryos (Supplementary Fig. S2B). Immunoblotting with a peptide-directed antibody raised against the C-terminal sequence DRVSYQPVDLRAAPLHRS of FtsH12 revealed steady abundance of this protease during leaf development, not only in chloroplasts, but also in non-photosynthetic organs, including roots (Supplementary Fig. S3A). In

dark-grown A. thaliana cell cultures, where chloroplast development is delayed due to the lack of leaf tissue (Dubreuil et al., 2018), FtsH12 was detected in proplastids, throughout all stages of plastid development and in mature chloroplasts (Supplementary Fig. S3B).

Based on limited cleavage by thermolysin in the protease protection assays with isolated pea chloroplasts, FtsH12 was reported to be located in the inner chloroplast envelope (Li et al., 2017). However, thermolysin has been reported not to penetrate the outer chloroplast envelope (McAndrew et al., 2001; Knopf et al., 2012); limited cleavage would therefore indicate a localization in the outer chloroplast envelope. This ambiguity led us to reinvestigate biochemical fractions of chloroplasts. Compared with whole chloroplast extracts, the FtsH12 immunosignal strongly increased in envelope fractions, but was absent in samples of the thylakoid membrane (Supplementary Fig. S4A). The orientation of FtsH12 within the envelope membrane was further tested in organello protease protection assays. Treatment with thermolysin only slightly decreased the amount of mature FtsH12 (Supplementary Fig. S4B), most likely due to the presence of broken chloroplasts. In contrast, treatment of intact chloroplasts with trypsin, which is able to penetrate the outer envelope (McAndrew et al., 2001), removed the protein band detected at 112 kDa. Both treatments lead to new digestion products with molecular masses of 60 kDa, consistent with a C-terminal fragment after truncation before the second transmembrane domain. Peptide competition demonstrated that these bands were specific for the FtsH12 epitope (Supplementary Fig. S4C). After solubilization of the membranes with Triton X-100, FtsH12 was completely degraded by both thermolysin and trypsin (Supplementary Fig. S4B). Together, this confirms that FtsH12 is located in the inner chloroplast envelope, with the C-terminal part containing the AAA-type domain and the catalytic domain facing the stroma, as previously suggested by Li et al. (2017) and confirmed by Schreier et al. (2018).

FtsH12 forms a heteromeric complex with inactive FtsH subunits and plastid NAD-malate dehydrogenase

Homozygous ftsh12 knock-out lines arrest embryo development at the heart stage (Meinke et al., 2008). To determine native interaction partners of FtsH12, we generated a stable insertion line expressing FtsH12 MYC-tagged at its C-terminus under control of the native FtsH12 promoter (P12::ftsH12CDS::4×c-myc; Supplementary Fig. S5) in the background of a mutant line carrying a T-DNA insertion in the seventh exon of FTSH12. Expression of MYC-tagged FtsH12 allowed segregation of a viable homozygous ftsh12 T-DNA insertion line with no visible phenotype, indicating full complementation and a normal function of MYC-tagged FtsH12. FtsH12 complexes were isolated from chloroplasts of homozygous P12::ftsH12CDS::4×c-myc plants lacking

endogenous FtsH12, by immunoprecipitation with anti-MYC antibody attached to magnetic beads and analyzed by mass spectrometry. As negative controls, pull-down experiments were performed with a MYC-tag using wild type chloroplasts, and pull-down by His-tag using the pFTSH12::FTSH12::6×Myc lines (Supplementary Fig. S6). Proteins with annotated chloroplast location identified in both biological replicates, but not the control samples, were considered as strong candidate interaction partners, and are shown in Table 1. FtsH12 was identified with most unique peptides and strongest intensity, followed by plastid malate dehydrogenase, FtsHi1, and FtsHi5. Additionally, two ribosomal proteins co-immunoprecipitated strongly with FtsH12 (Table 1). Also, FtsHi2 and FtsHi4 co-immunoprecipitated with FtsH12, but failed to meet our criteria as they were only detected in one of the two replicate experiments with P12::ftsH12CDS::4×c-myc (Supplementary Table S2). Nevertheless, this indicates that all four FtsHi homologs and pdNAD-MDH form a complex with FtsH12 (Schreier et al., 2018), even when FtsH12 is expressed under its native promotor, whereas we did not detect YCF2 after immunoprecipitation of FtsH12 expressed under its native promoter and the chosen isolation conditions.

To analyse if the presence of the inactive FtsHi enzymes had impact on the FtsH12/FtsHi1,2,4,5 complex accumulation, FtsH12 was immuno-stained in the heterozygous *FTSHi* mutants *ftshi2*/FTSHi2-5, *ftshi4*/FTSHi4-1 and *ftshi5*/FTSHi5-1 (Mishra *et al.*, 2019), as well as in the homozygous mutants *ftshi1* and *ftshi4-2* (Mishra *et al.*, 2019), and their respective wild type controls (Fig. 1; Supplementary Table S3). While the amount of FtsH12 seemed to be similar in wild type and the heterozygous mutants, in *ftshi1* the amount of FtsH12 was strongly up-regulated. In *ftshi4-2*, however, the amount of FtsH12 was slightly diminished.

Reduced amount of FtsH12 cause changes in leaf phenotype, pigmentation and plastid ultrastructure

To gain insights into the physiological functions of FtsH12, we generated micro-RNA lines with reduced amounts of FtsH12, as well as FTSH12 overexpressor lines (S35::ftsH12CDS) in A. thaliana Col-0 background. Two independent homozygous FTSH12 overexpressor lines (ox12-1, ox12-2) and three independent micro-RNA lines (indicated as mi12-1, mi12-2 and mi12-3 in the protein domain structure of Supplementary Fig. S1A) were selected for further experiments. Immunoblot analyses using the FtsH12 antibody showed a reduction of FtsH12 in all mi12 lines by 50-60% compared with that seen in wild type, while ox 12 lines showed increased amounts of FtsH12 by 200-400% compared with wild type grown in short day conditions (Fig. 2A), independent of the age of plants or leaves. Strong phenotypic differences were observed in the FTSH12 knock-down plants: Two days after germination in light, the mi12 lines displayed pale yellow cotyledons (Fig. 2B, upper panel), in which chlorophyll accumulation was retained. In nine-week-old plants of mi12 lines, a variegation pattern of light yellow-green and dark green areas was observed in young developing leaves, while mature leaves contained almost no variegated areas (Fig. 2B, lower panel). Consistently, significantly reduced Chl a and Chl b content was found in young mi12 leaves (Supplementary Fig. S7C). Mature mi12 plants appeared slightly smaller, but this difference in their rosette size was not significant (Supplementary Fig. S7A). Furthermore, their cotyledon tip-to-tip distance was significantly reduced compared with the wild type (Supplementary Fig. S7B). Maximal PSII quantum yields and non-photochemical quenching in fully developed leaves of mi12 lines were indistinguishable from wild type (Supplementary Table S4). In contrast to FTSH12 knock-down, ox12 lines with increased

Table 1. Stringent subset after immuno co-precipitation of myc-tagged FtsH12 expressed under its native promoter. Two independent experiments were performed on two FtsH12-4x-cMYC expressing lines, proteins were identified and quantified by LC-MS/MS; only putative interactors observed in both replicate pull down experiments are shown. UniProt-annotated names and accession numbers, number of unique peptide sequences found for each protein group, sequence coverage in percent, and log₂ transformed MaxQuant LFQ intensity for each experiment are listed.

| Names | UniProt ID | Unique peptides | Sequence coverage [%] | log₂(LFQ) FtsH12-4xcmyc replicate 1 | log₂(LFQ) FtsH12- 4xcmyc replicate 2 |
|---|----------------|--------------------|-----------------------|--|---|
| FtsH12-4xcMYC | | 12 | 13.7 | 20.7 | 19.1 |
| Malate dehydrogenase, chloroplastic | Q9SN86 | 7 | 23.8 | 18.9 | 20.5 |
| 50S ribosomal protein L12,chloroplastic | P36212; P36210 | 3 | 36.4 | 18.5 | 20.5 |
| 30S ribosomal protein S19, chloroplastic | P56808 | 2 | 20.7 | 17.0 | 19.2 |
| Inactive ATP-dependent zinc metalloprotease FtsHi5 | F4J3N2 | 4 | 5.1 | 16.3 | 19.5 |
| Inactive ATP-dependent zinc metalloprotease FtsHi1 | O22993 | 7 | 10.3 | 19.0 | 16.4 |

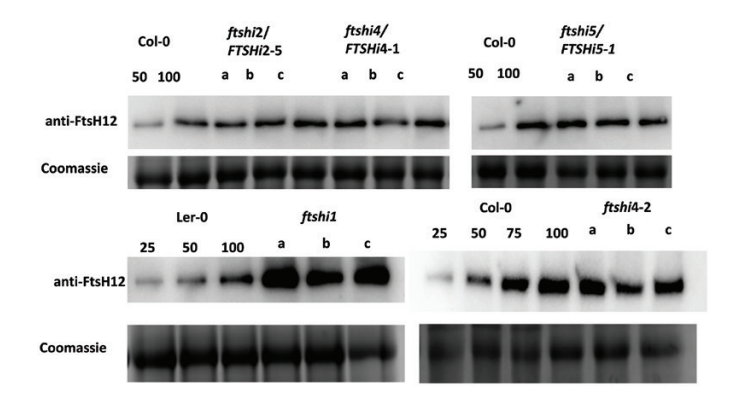


Fig. 1. Expression of FTSH12 in T-DNA inserted FTSHi mutant lines. Immunostaining of FtsH12 in total protein extracts of 10 day-old FTSHi mutant seedlings grown on MS-media growth plates. FtsH12 protein amount is displayed in the heterozygous mutants ftshi2-5, 4-1 and 5-1 (upper panel) and in the homozygous mutants ftshi1-1 and ftshi4-2 (lower panel). Information on the FTSHi mutant lines can be found in (Mishra et al., 2019). A total of 15 µg protein was loaded from the FTSHi mutant lines and wild type (100%); for comparison wild type was additionally loaded at lower concentrations (25, 50, and 75%). a, b, c correspond to three biological replicates.

amounts of FtsH12 showed larger cotyledon tip-to-tip distance and higher chlorophyll content in mature leaves, but none of these apparent differences were significant compared with wild type (Supplementary Fig. S7A, B and Table S4). No obvious changes in superoxide anion or hydrogen peroxide concentrations were observed in 10-day-old wild type or mutant seedlings grown either in short day or in continuous light (Supplementary Fig. S8).

To analyse if FTSH12 overexpression had the potential to accelerate chloroplast development, wild type and FTSH12 mutant lines were exposed to de-etiolation; under these more challenging conditions FTSH12 overexpression might provide an advantage (Fig. 3A; Supplementary Fig. S7D, E). The FTSH12 knock-down lines mi12-1 and mi12-2 remained smaller (Supplementary Fig. S7E), accumulated anthocyanins (Supplementary Fig. S7D), and therefore had a pink appearance (Fig. 3A). Interestingly, the overexpressor lines contained significantly more chlorophyll during day 1 and day 2 of de-etiolation than wild type (Fig. 3B, right panel).

Chloroplasts of two-day-old seedlings of wild type, overexpressor (ox12-1, ox12-2) and knock-down (mi12-3) lines were isolated and their sizes analysed in isosmotic medium by light microscopy (Fig. 4A). In addition the morphology of chloroplasts in variegated leaf areas of young (12 d) and old (nine weeks) mi12 plants (Fig. 4B, C) were analysed by transmission electron microscopy (TEM). While wild type and the overexpressor lines displayed length/width (l/w) ratios of 1.4 and 1.5, chloroplasts isolated from mi12 were more spherical with a significantly lower l/w ratio of 1.1. Also the average diameter of chloroplasts in the FTSH12 knock-down mutant was significantly reduced to 3.3 μm, compared with 4.3 μm in wild type and ox 12 lines (Fig. 4D). In the TEM analysis, wild

type chloroplasts displayed a l/w ratio of 2.2, while chloroplasts of the mi12-3 line had a l/w ratio of 1.5, confirming the results obtained by light microscopy (LM) of isolated chloroplasts (Fig. 4D). Furthermore, a smaller fraction of the thylakoid membranes in the FTSH12 knock-down plants appeared stacked into grana lamellae, with fewer and lower stacks compared with wild type. Irrespective of the plant age, the distances between the thylakoid membranes (stroma lamellae and grana stacks) seemed enlarged in mi12-3 (Fig. 4B, C).

Altered FtsH12 amounts affect translocon at the inner chloroplast envelope membrane composition

To obtain a global view on differences in protein abundance, proteomes extracted from four biological replicates of twoday-old wild type, ox 12-1 and mi12-3 seedlings were analysed. Label-free quantitative mass spectrometry was used to identify 4061 proteins, of which 3129 could be quantified in at least two replicate experiments of one genotype (Supplementary Table S5). This included FtsH12, which showed modest abundance in wild type, massive accumulation in the overexpressor line, and abundance below detection limit in the miRNA line, as judged by intensity-based absolute quantification (iBAQ) values (Table 2). Note that the relative FtsH12 amounts suffer from a bias, as only a single FtsH12 peptide was quantified in wild type, but 14 were quantified in the overexpressor line, resulting in higher summed intensity and exaggerated iBAQ. Given the proposed function of FtsH12 as part of an import motor protein complex, we further analysed the behavior of the FtsH12complex subunits, TIC components and other importassociated proteins identified in our dataset, as summarized in Table 2. The FtsHi subunits reflected FtsH12 amounts and were not detected in mi12-3, but significantly accumulated in ox12-1. YCF2 was significantly reduced in mi12-3, but not up-regulated in ox12-1, while the amount of the abundant plastidial NAD-MDH did not differ in mi12-3 and wild type. Subunits of the 1 MDa TIC complex comprising Tic100, Tic56, YCF1/Tic214 and Tic20-I (Nakai, 2018), that has been shown to interact with the FtsH12 complex (Kikuchi et al., 2018), appeared to accumulate in mi12-3 compared with wild type. Notably, a complementing trend was reported for depletion of Tic56, which increased the abundance of the FtsH12 complex (Schäfer et al., 2019). Amongst the other identified TIC subunits, only TIC22-III showed significant accumulation in mi12-3 compared with wild type, whilst all other identified TIC subunits and chaperones considered as plastid import motor components accumulated only in ox12-1 compared with wild type (Table 2). To investigate the cause of these striking changes in TIC complex subunit abundance, we next analysed RNA extracted from two day- and six-week-old Arabidopsis leaves by qPCR (Supplementary Fig. S9). In 2 d-old seedlings, the



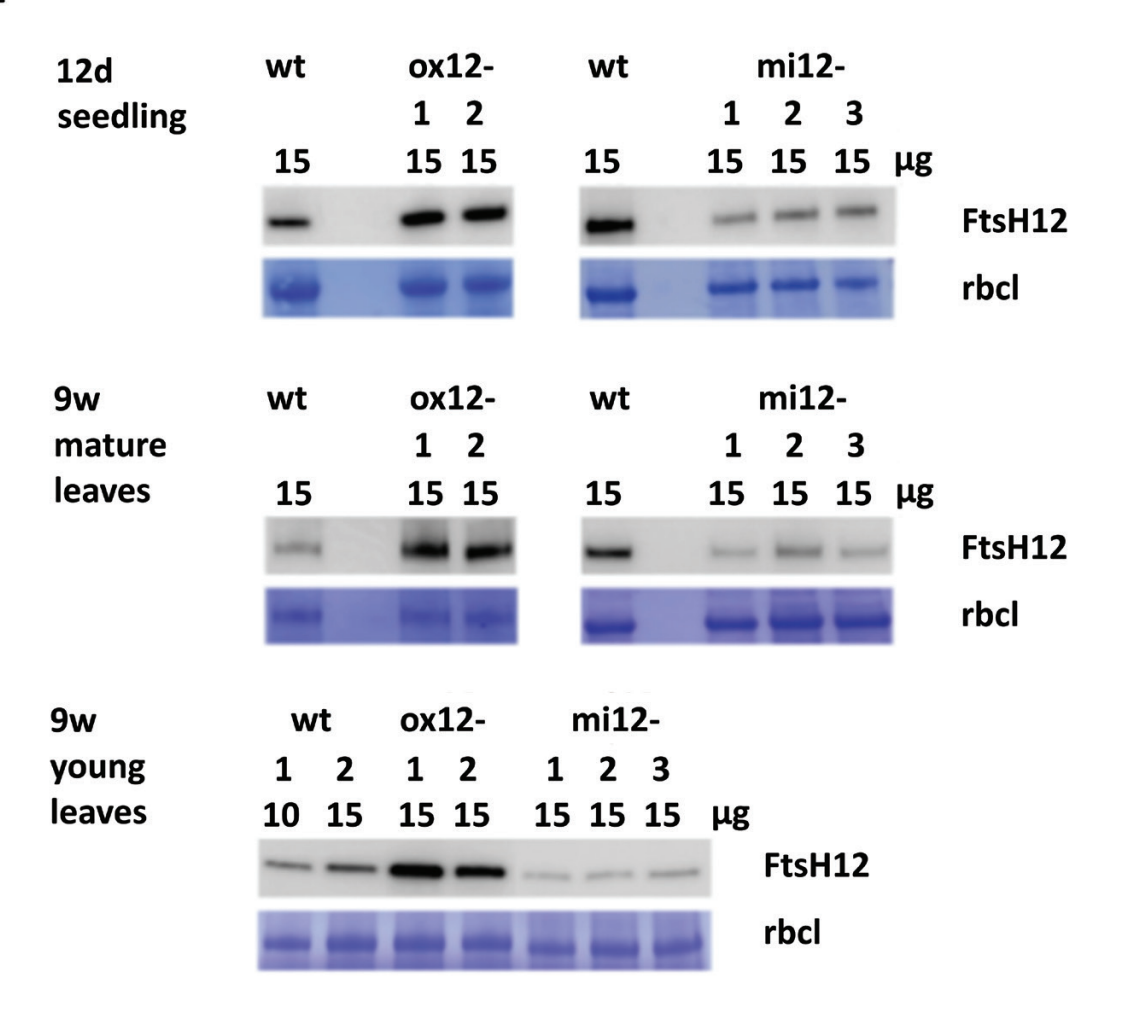




Fig. 2. Phenotypic comparison of wild type (WT), *FTSH12* overexpressor and knock-down plants. (A) Immunostain to quantify FtsH12 protein amounts in leaves of wild type and independent transgenic lines at 12 days (12 d) and nine weeks (9 w) of age grown in short light regime (8 h of light per day). Rosette leaves of nine-week-old plants were analysed separately for developing (young) and mature leaves. Amounts of total proteins loaded on SDS PAGE are given above each lane. At least three biological replicates were tested. As loading control the Coomassie-stained band of large subunit of RuBisCo (rbcL) is shown. (B) Phenotypes of *A. thaliana* wild type and transgenic lines with increased (*ox12-1* and *ox12-2*), or reduced (*mi12-2* and *mi12-3*) *FTSH12* expression grown in short day light regime (8 h of light per day). Two-day-old seedlings are shown in the upper panel (scale bar represents 1 mm), and leaves of nine-week-old plants in the lower panel (scale bar represents 1 cm).

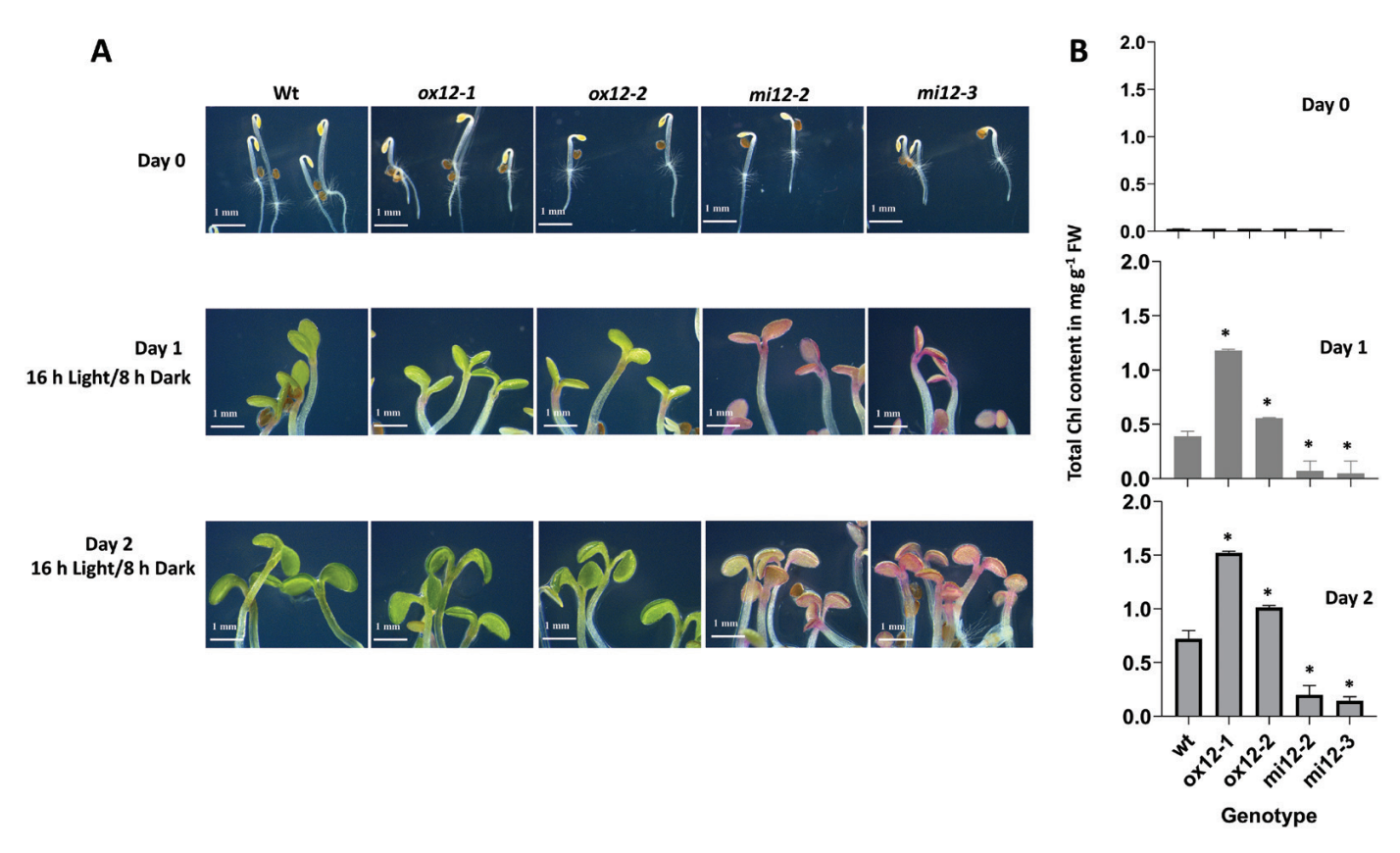


Fig. 3. De-etiolation of wild type (WT). FTSH12 overexpressor and knock-down plants. (A) Greening of wild type and transgenic lines (ox12-1, ox12-2 and mi12-2, mi12-3) after etiolated growth (0 h light, top panel) for five to six days followed by illumination (16 h light/8 h dark) for 1 d (middle panel) and 2 d (bottom panel). Scale bar=1 mm. (B) Quantification of chlorophyll content in wild type and mutant lines during de-etiolation. Significant differences between wild type and transgenic plants are indicated by asterisk (Student's t-test, P < 0.05).

transcripts of YCF1, TIC100, and TIC56, as well as TIC110 and TIC40, were strongly up-regulated in the overexpressor line ox12-1 compared with wild type, but also, to a lesser extent, in the knock-down line mi12-3. In leaves of sixweek-old plants, however, only mi12-3 expressed TIC100, TIC110 and TIC40 stronger than wild type, while expression of all complex subunits was reduced in ox12-1 compared with wild type. Taken together, these results suggests that FtsH12 abundance determines the accumulation of the FtsH12-FtsHi-pNAD-MDH complex, and further affects the abundance of the 1 MDa TIC complex by transcriptional changes.

Seedlings with modulated FtsH12 content show drastic changes in proteome composition

The quantitative proteome analysis further indicated massive changes in proteome composition in FTSH12 transgenic plants, with 1450 of the 3129 quantified proteins exhibiting significant differences in abundance (ANOVA with Benjamini-Hochberg FDR < 0.05, followed by Tukey's honest significance test; Benjamini and Hochberg, 1995; Supplementary Tables S5 and S6). Principal component analysis (PCA) clearly separated the data into three distinct clusters representing wild type, mi12-3, and ox12-1, verifying that the observed changes were indeed linked to the genotypes (Fig. 5A). Hierarchical clustering of z-score normalized intensities of proteins with differential abundance revealed seven clusters with similar protein accumulation profiles (Fig. 5B, C, Supplementary Table S5); these were further analysed for enriched KEGG functional categories and known interactions among the cluster constituents, using the String database (Szklarczyk et al., 2018). The large cluster 1 contained 514 highly connected proteins with lower abundance in ox12-1 compared with wild type and miRNA knock-down (Fig. 5C). KEGG term enrichment indicated that this cluster included many of the proteins involved in central carbon metabolism or protein synthesis and quality control, such as the spliceosome, ribosome, proteasome and reticulum proteins (Supplementary Fig. S10). Cluster 2 consisted of 256 proteins with higher accumulation in mi12-3, but no significant difference between ox12-1 and wild type, which included additional proteasomal subunits, proteins involved in carbon metabolism, and phagocytosis (Supplementary Fig. S11). Also, proteins involved in fatty acid metabolism, such as acetyl coenzyme A carboxylase 1 (ACC1) and fatty acid export 1 (FAX1), and the translocon on the outer chloroplast membrane (TOC) 34,

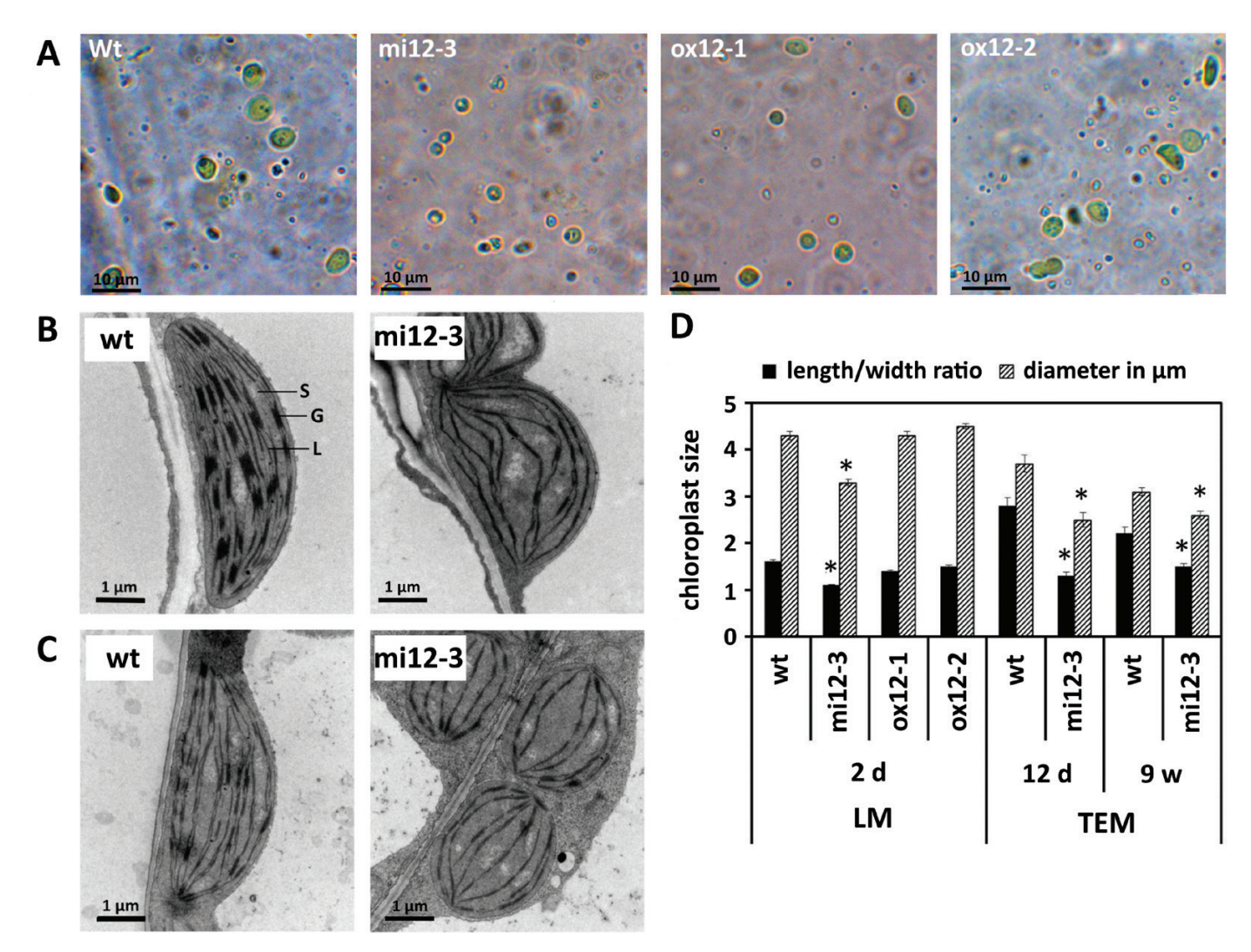


Fig. 4. Size and morphology of chloroplasts. (A) Light microscope (LM) micrographs of isolated chloroplasts of two-day-old wild type (WT) seedlings and *FTSH12* mutant lines in isosmotic buffer visualized with a Zeiss Axioplan 2 at 1000 × magnification. (B, C) Transmission electron micrographs (TEM) showing chloroplasts of wild type and of the *FTSH12* knock-down line (*mi12-3*, variegated leaf areas) at the age of 12 d (B) and nine weeks (C). Visible are the chloroplast stroma (S) containing the thylakoid membrane consisting of dense photosystem II-containing grana stacks (G) and photosystem I-enriched stroma lamellae (L). (D) Average diameters (grey bars, ±SE) and length to width ratios (black bars, ±SE) of chloroplasts are shown for each genotype. Significant differences compared with wild type are indicated by an asterisk (n>35 for light microscope pictures, n>15 for TEM, *P*<0.05, Student's *t*-test).

translocon on the inner chloroplast membrane (TIC) 22L and 110 and the chloroplastic import inner membrane translocase subunit HP30-2, components of the plastid protein import machinery, were found in this cluster (Supplementary Table S5). Notably, clusters 1 and 2 together contained 75 proteins that are commonly observed in albino/green pale mutants, indicating general proteome changes associated with impaired photosynthesis (Motohashi *et al.*, 2012). A small cluster 3 contained 38 proteins with reduced abundance in *mi12-3*, compared with the other two genotypes, including YCF2, but it was too heterogeneous to reveal enriched KEGG terms.

GO term analysis showed the presence of a small cluster of four RNA helicase-associated proteins (Supplementary Fig.

S12). Cluster 4 consisted of 135 proteins that were less abundant in both *FTSH12* mutants, *oxp12-1* and *mi12-1*, compared with wild type. This cluster included 20 subunits of the cytosolic ribosome complex (Supplementary Fig. S13). Cluster 5 contained 121 proteins with higher abundance in both *FTSH12* mutants, including an additional nine ribosomal proteins (Supplementary Fig. S14), but also the plastid RNA polymerase subunits RPOA and RPOB. Cluster 6 contained 279 proteins with highest abundance observed in *ox12-1*, and lowest abundance in *mi12-3*, and therefore correlated with the amount of FtsH12. This cluster was formed by chloroplast proteins highly connected with each other in the graphical depiction (Supplementary Fig. S15), and with KEGG-annotated functions in photosynthesis, photosynthetic

Downloaded from https://academic.oup.com/jxb/article/72/9/3455/5995586 by Forschungszentrum Juelich GmbH, Zentralbibliothek user on 06 May 2021

Table 2. Comparison of FtsH12 and TIC complex protein abundance in FTSH12 mutants. Protein abundance in FtsH12 knock-down plants (mi12-3), overexpressors unique peptides supporting the identification, and average iBAQ values as a measure of protein abundance. Significance between FTSH mutants and wild type was (0x12-1) and wild type (MT) was determined by label-free mass spectrometry. Listed are protein names with gene loci and associated Uniprot IDs, number of determined by a two-tailed Student's t-test (P<0.05)

| Protein name | Gene loci | UniProt IDs | Unique peptides | Average iBAQ mi12-3 | Average iBAQ WT | Average iBAQ ox12-1 | Significant WT/mi12-3 | Significant ox12-1/mi12-3 | Significant ox12-1/WT |
|-------------------------------|--|---------------|--------------------|---------------------|--------------------|---------------------|--------------------------|---------------------------|-----------------------|
| FtsH12 motor complex subunits | olex subunits | | | | | | | | |
| FTSH12 | At1g79560 | Q9SAJ3 | 41 | 0 | 3110 | 87 893 | + | + | + |
| FtsHi1 | At4g23940 | 022993 | 9 | 0 | 2134 | 8014 | + | + | + |
| FtsHi2 | At3g16290 | A8MPR5 | 4 | 0 | 3824 | 8437 | + | + | + |
| FtsHi4 | At5g64580 | F4KF14 | က | 0 | 3992 | 6308 | + | + | + |
| FtsHi5 | At3g04340 | F4J3N2 | 2 | 0 | 629 | 2509 | | + | + |
| YCF2 | AtCg00860;AtCg01280 | P56786 | 2 | 1433 | 2470 | 1453 | + | | |
| pdNAD-MDH | At3g47520 | 09SN86 | 13 | 1 270 450 | 1 093 783 | 1 718 300 | | + | + |
| 1MD TIC complex | | | | | | | | | |
| TIC214 / YCF1 | AtCg01000;AtCg01130 | P56785 | 14 | 20 821 | 2005 | 19 452 | + | | + |
| TIC100 | At5g22640 | Q8LPR8 | 7 | 16 646 | 3752 | 33 105 | + | | + |
| TIC56 | At5g01590 | Q7Y1W1 | 9 | 19 101 | 7802 | 46 503 | | | + |
| Other TIC subunits | | | | | | | | | |
| TIC110 | At1g06950 | Q8LPR9 | 43 | 568 540 | 396 450 | 667 520 | | | + |
| TIC40 | At5g16620 | Q9FMD5 | 9 | 105 910 | 83 516 | 123 841 | | | + |
| TIC62 | At3g18890 | Q8H0U5 | 9 | 0 | 0 | 23 804 | | + | + |
| TIC55 | At2g24820 | Q9SK50 | 00 | 10 723 | 8683 | 40 684 | | + | + |
| TIC22-IV | At4g33350 | Q9SZB2 | 2 | 29 746 | 24 446 | 49 074 | | + | + |
| TIC22-III | At3g23710 | F4J469 | 2 | 20 041 | 5375 | 10 095 | + | + | |
| Chloroplast chapen | Chloroplast chaperones with suggested motor function | ınction | | | | | | | |
| cpHsc70-1 | At4g24280 | Q9STW6 | 0 | 1 728 700 | 1 531 400 | 2 821 950 | | + | + |
| cpHsc70-2 | At5g49910 | Q9LTX9 | 6 | 188 855 | 207 958 | 395 635 | | + | + |
| HSP93-III/ | At3g48870 | F4JF64;Q9SXJ7 | 12 | 176 430 | 168 343 | 250 565 | | + | + |
| CLPC2 | | | | | | | | | |
| CLPC1 | At5g50920 | Q9F156 | 13 | 1 257 550 | 1 220 073 | 2 193 150 | | + | + |
| | | | | | | | | | |

carbon fixation, chlorophyll biosynthesis, and plastid protein synthesis. Finally, cluster 7 contained 107 proteins with distinctly higher abundance in *ox12-1* compared with wild type and *mi12-3*, including many thylakoid proteins, the plastid envelope and stromal proteins TIC62, TIC55, YCF3, and chlorophyll synthase (Supplementary Table S6), and also subunits of the plastid ribosome (Supplementary Fig. S16). Taken together, clusters 6 and 7 reflected the accelerated development of photosynthetic capacity in *ox12-1* and wild type, compared with *mi12-3* seedlings observed at this stage.

N-terminome analysis shows normal maturation of plastid-imported proteins in FtsH12 mutants

Given the reduced abundance of nuclear-encoded, plastid-imported proteins, we considered whether altered FtsH12 abundance would result in differential processing of nuclear-encoded proteins after plastid import. To address this problem, we profiled N termini of proteins in the same samples using undecanal-assisted N-termini enrichment, in an early version

of our recently published HUNTER protocol (Weng et al., 2019). Free primary amines, including α -amines of protein N-termini generated by in vivo proteolytic processing, were modified by reductive dimethylation using distinct formaldehyde isotopes for each line. Tryptic digest then generated new primary amines on non-N-terminal peptides that were subsequently tagged with long-chain hydrophobic aldehyde, allowing their removal from both endogenously modified and in vitro dimethylated N-terminal peptides by reversephase C18 solid phase extraction. Mass spectrometric analysis identified 1292 N-terminal peptides from 498 proteins, including 592 N-terminal peptides modified by endogenous N-terminal acetylation and 700 dimethylated peptides representing N termini with free α -amines in vivo (Supplementary Table S7). Positional annotation revealed that the majority of the N-terminal peptides matched the protein start site with intact or excised initiator Met, positions within five amino acids distance from sites of signal peptide cleavage in the secretory pathway, or transit peptide cleavage after import into mitochondria or chloroplasts, as predicted by TargetP2.0 (Almagro

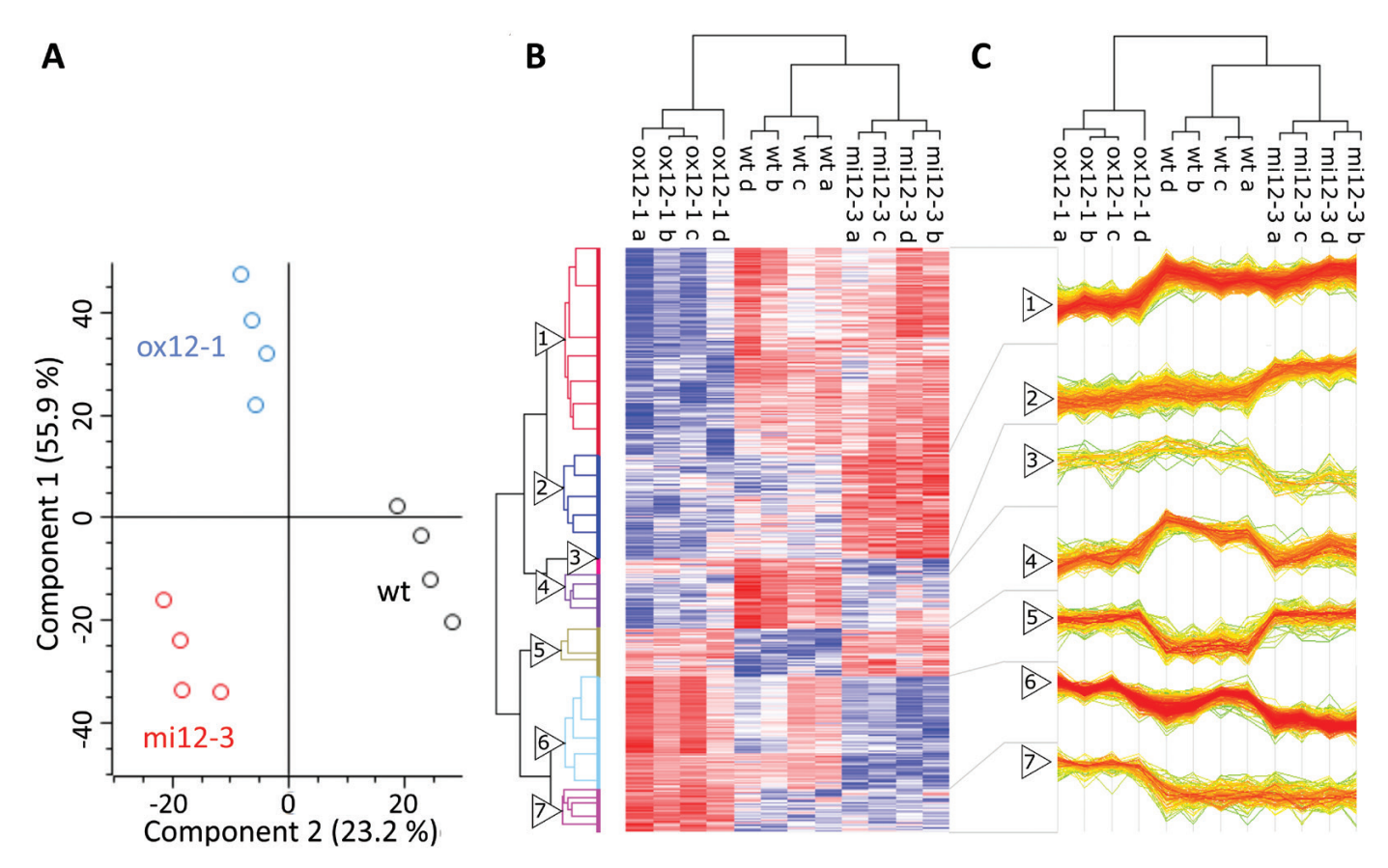


Fig. 5. Label free quantitative proteome analysis of two-day-old wild type (WT), ox12-1 and mi12-3 seedlings. (A) Principal component analysis (PCA) of 1450 proteins with significant differences in abundance between the three lines. Four biological replicates were analysed for each line, differences determined by multi-sample ANOVA with Benjamini-Hochberg correction for multiple hypothesis testing (FDR<0.05). WT: Black circles, mi12: red circles, ox12: blue circles. (B) Hierarchical clustering of the 1450 proteins with significant differences in abundance after Z-score normalization. Blue color of the heat map indicates LFQ intensities below, and red color, above average for each protein. (C) Expression patterns of the seven clusters with similar protein abundance profiles determined by hierarchical clustering in (B), with more intense red indicating larger number of overlaying expression profiles.

Armenteros et al., 2019; Fig. 6A). Of all identified N-terminal peptides, 343 (27%), including 91 peptides from proteins with predicted plastid TP (Transit peptide), matched to sites within the protein models that have not been previously annotated (Fig. 6A). As expected, the majority of the N-terminal peptides at positions 1 (89%) and 2 (78%) were N-terminally acetylated, as were a large proportion (27%) of the mature plastid N-termini. However, only few mitochondrial protein N-termini, and none of the signal peptide-processed N-termini were N-terminally acetylated. Out of the unannotated N-terminal peptides, 43 were acetylated, which indicates proteoforms arising from alternative splicing, use of alternative translation initiation sites, or rare post-translational N-terminal acetylation after proteolytic processing (Perrar et al., 2019).

To determine significantly altered protein termini abundance that may indicate differential cleavage between two genotypes, we filtered the dataset for N-terminal peptides changing more than 50% in abundance (log₂ (FC)>0.58 or <-0.58) that were supported by a LIMMA-moderated t-test (P-value<0.05; Gomez-Auli et al., 2016; Hartl et al., 2017). Application of these criteria to compare plants with highest and lowest abundance of FtsH12 identified 86 N-terminal peptides with significantly higher abundance in ox12-1 than in mi12-3 (Fig. 6B; Supplementary Table S7), of which 69 belonged to 62 plastid proteins. Expected positions at the translation start site of plastid-encoded proteins or predicted TP cleavage sites were matched for 53 significantly changing N-terminal peptides, which included the mature dimethylated N-terminus of FtsH12 starting at Ser51 after TP cleavage (Fig. 6B). In contrast, 29 N-terminal peptides, including only six from plastid-imported proteins, were more abundant in the knock-down mi12-3 compared with the overexpressor line ox12-1 (Fig. 6C). Comparison of wild type with mi12-3 (Supplementary Fig. S17A), and ox12-1 with wild type revealed similar results (Supplementary Fig. S17B). Thus, both expected and unexpected plastid protein N-termini were consistently more abundant in the plant line with higher FtsH12 content in each comparison. Consistently, we observed a significant correlation between N-termini abundance and the corresponding total protein abundance determined by label-free quantitation in all three comparisons of ox 12-1 and mi12-3 (Pearson correlation r=0.67; Fig. 6C), mi12-3 and wild type (r=0.61; Supplementary Fig. S17C) and ox 12-1 and wild type (r=0.70; Supplementary Fig. S17D). This indicated that the majority of the changes in N-termini abundance reflected the changes in overall proteome composition. A few N-terminal peptides showed deviating behavior, with significant changes in ox12-1 or wild type compared with mi12-3, and unchanged protein abundance. However, on manual inspection these were found either not to be plastid-located and/or arising from low abundance proteins, where imputation compressed or masked the true protein

ratio in the proteome dataset. Therefore, no strong candidates for direct FtsH12-mediated proteolytic cleavage were observed. We further speculated that altered FtsH12 activity might alter protein maturation after import. Most of the identified N-termini of nuclear-encoded plastid-targeted proteins matched chloroplast TP cleavage sites predicted by TargetP2.0, or were shifted by one or two residues towards either site (Fig. 6D), while N-terminal peptides resulted from proteolytic cleavage within the protein. The latter may reflect functional processing, for example, the eight identified lumen TP cleavages (Supplementary Table S7), or represent degradation intermediates of abundant proteins. Similar "ragged" plastid protein N-termini and proteolytic fragments have previously been observed by detailed plastid N-terminome profiling (Rowland et al., 2015). Only 25 N-terminal peptides of plastid proteins matched to positions more than five amino acids preceding the predicted transitpeptide cleavage sites, including 12 N-termini mapping to position 2 of the protein model, indicating intact full-length precursor proteins (Supplementary Table S7). All of these were N-terminally acetylated at P2 after Met removal, but only the N-terminal peptide of an uncharacterized precursor protein encoded by gene At4g28440 contained a labeled Lys residue that allowed quantification in our assay, but was not significantly altered between the mutants.

Discussion

Seed development of homozygous ftsh12 knock-out plants is known to arrest at the heart stage of development (Meinke et al., 2008). Consistent with an important general function in plastids and plastid development, we have shown that FTSH12 is expressed throughout chloroplast development in synchronized cell cultures (Supplementary Fig. S3B), and also in non-photosynthetic proplastids and roots (Supplementary Fig. S3A). Biochemical fractionation of isolated chloroplasts further demonstrated that FtsH12 resides in the inner chloroplast envelope (Supplementary Fig. S4). In a previous study, FtsH12 was synthesized in vitro and imported into isolated pea chloroplasts (Li et al., 2017). Subsequent treatment with thermolysin, a protease reported to be unable to penetrate the outer chloroplast envelope membrane (Knopf et al., 2012), yielded a 39 kDa FtsH12 fragment, which would suggest that both N- and C-termini of FtsH12 protrude into the cytosol. In our assays, an antibody directed against the C-terminus of FtsH12 immuno-stained a band of 60 kDa after treatment with trypsin (Supplementary Fig. S4), a protease that penetrates the outer envelope membranes (McAndrew et al., 2001). To some extent, the same fragment was observed after thermolysin treatment, presumably due to the presence of plastids with disrupted outer envelopes. FtsH12 was completely degraded by both proteases when detergent was added, suggesting that its

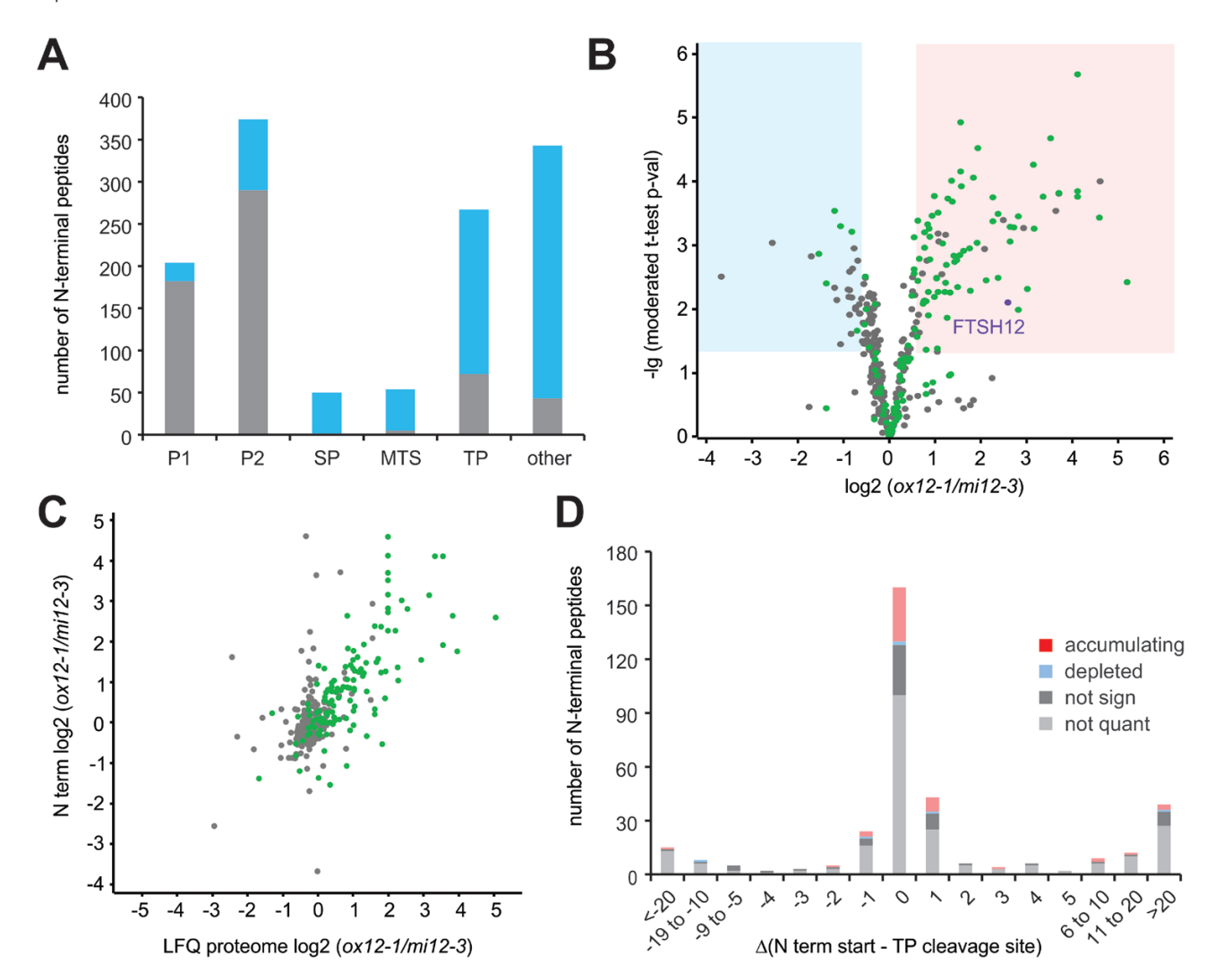


Fig. 6. Quantitative N-terminome analysis in *FTSH12* mutants compared with wild type. (A) Positional annotation of 1292 identified N-terminal peptides. Peptides mapping to translation start sites with intact or excised initiator-Met (Pos1/2) or within five amino acids of TargetP2.0 annotated as signal peptide, plastid or mitochondrial transit peptide or propeptide maturation sites, were defined as 'expected' N termini. Light grey, peptides with endogenous N-terminal acetylation; dark grey, peptides *in vitro* marked by dimethylation, indicating *in vivo* free N-terminal amines. (B) Volcano plots of N-terminal peptide abundance in *ox12-1* compared with *mi12-3*. Peptides from plastid-located proteins (plastid encoded or predicted to target to the plastid by TargetP2.0) are highlighted in green. N-terminal peptides with significantly reduced or increased abundance (Student's *t*-test *P*-value<0.05 and log₂ FC<-0.58 or >0.58) are highlighted with blue and red color background. (C) Comparison of N-terminal peptide abundance with the corresponding protein abundance within *ox12-1* and *mi12-3*. Peptides from plastid proteins are highlighted in green. Pearson correlation coefficient with confidence level is indicated. (D) Comparison of the position of plastid protein N-terminal peptides to the transit peptide cleavage predicted by TargetP2.0. Protein termini showing significant accumulation or depletion change in *ox12-1* compared with *mi12-3* are highlighted in red and blue, respectively. Dark grey indicates unaltered abundance, light grey indicates peptides not quantified in two or more replicates.

catalytic and ATPase domain face the stroma, in agreement with more recent similar data (Kikuchi *et al.*, 2018; Schreier *et al.*, 2018). Together, this unambiguously confirms the localization of FtsH12 in the inner chloroplast envelope, as suggested previously (Li *et al.*, 2017). The observed sensitivity of FtsH12 to thermolysin treatment after *in vitro* import into pea chloroplasts (Li *et al.*, 2017), contrary to the expected behavior of inner envelope proteins in these assays (McAndrew *et al.*, 2001; Knopf *et al.*, 2012), may be due to (i) incorrect integration of pre-FtsH12, (ii) partially disrupted outer envelope, or

(iii) a different resistance to thermolysin penetration in pea compared with Arabidopsis chloroplasts.

Complementation of an embryo-lethal *FTSH12* T-DNA insertion line allowed us to segregate a mutant line solely by expressing Myc-tagged FtsH12 under its native promoter. We used this line to study the native FtsH12 interaction partners without the presence of potentially interfering wild type protein, or side effects arising from overexpression. In two independent experiments, we were able to pull-down FtsH12 together with FtsHi1, FtsHi5, and the plastidic form of MDH

from isolated chloroplasts, with FtsHi2 and FtsHi4 additionally found in one experiment (Supplementary Table S2). This is in agreement with data obtained by others, where a heteromeric complex comprised of FtsH12, FtsHi1, FtsHi2, FtsHi4, FtsHi5, pdNAD-MDH, and YCF2 was identified in co-immunoprecipitation experiments using Arabidopsis plants expressing FtsH12 or pdNAD-MDG as YFP fusion proteins under the control of the 35S promotor (Schreier et al., 2018), and from tobacco chloroplasts expressing YCF2 as a HA-fusion protein (Kikuchi et al., 2018). This large heteromeric 2 MDa complex was further shown to associate with a TIC complex comprised of TIC20, TIC56, TIC100 and TIC214/YCF1, driving protein translocation by the pulling force generated by the ATPase domains of the FtsHi subunits (Kikuchi et al., 2018; Schreier et al., 2018). However, these studies did not determine the stoichiometry or subunit arrangement of the FtsH12 motor complex. In our hands, expression of FtsH12 was up-regulated in single knock-down FTSHi mutants at the transcript (Mishra et al., 2019) and protein (Fig. 1) level; in particular, the expression of FtsHi1 and FtsHi5 were dependent on the presence/absence of FtsH12. Both, FtsHi1 as well as FtsHi5 appeared most tightly bound to FtsH12 in our pull-down experiments (Supplementary Table S2). Given the strong expression of FtsH12 in the homozygous ftshi1 mutant, it is tempting to speculate that FtsH12 may be able to substitute for FtsHi1 in the protein complex.

To assess the effect of modulated FtsH12 abundance, we created transgenic miRNA knock-down lines with reduced FTSH12 expression (<40% of wild type), and overexpressor lines with increased FTSH12 content (>3× that in wild type; Fig. 2A). The most obvious and striking phenotype in our FTSH12 knock-down mutants were marbled (variegated) primary and young rosette leaves, dramatically altered chloroplast ultrastructure with deformed thylakoid membranes, and lower overall chlorophyll content. Similar pale-green or variegated phenotypes with altered chloroplast ultrastructure have also been observed in knock-down lines of FTSHi4, FTSHi5 (Lu et al., 2014; Wang et al., 2018) and pdNAD-MDH (Schreier et al., 2018), and in a line carrying a point mutation in ftshi1 that renders its ATPase domain inactive (arc1; Kadirjan-Kalbach et al., 2012; Mishra et al., 2019), consistent with an important function of the FtsH12 complex in chloroplast development (Kikuchi et al., 2018; Schreier et al., 2018). The arc1 mutant of FtsHi1 further contained smaller, more numerous chloroplasts, while overexpression of FTSHi1 resulted in fewer, but larger chloroplasts (Kadirjan-Kalbach et al., 2012). Similarly, a significant reduction in chloroplast size was observed in our FTSH12 knock-down plants (Fig. 4), but our FTSH12 overexpressor lines did not display significantly larger chloroplasts than wild type. Interestingly, when investigated under challenging conditions like de-etiolation (Fig. 3C), the overexpressor contained significantly more chlorophyll after one or two days in light, but did not grow faster. Even though phenotypic differences

between FTSH12 knock-down, wild type and overexpressor lines were most notable in early stages of plant development, we observed a delay of plastid development also during vegetative growth in developing leaves of FTSH12 knock-down lines, suggesting that the FtsH12 complex is important at all developmental stages. This is consistent with the observation of pale-green and variegated leaves after depletion of FTSHi5 by inducible expression of FTSHi5-targeting miRNA (Wang et al., 2018). However, these authors observed increased amounts of H₂O₂ in ftshi5-1, while in FTSH12 knock-down and overexpressor lines the occurrence of ROS was similar to wild type.

Mass spectrometry-based proteomics is the method of choice to determine the consequences of modulated protease activity at a molecular level (Demir et al., 2018). Quantitative proteomic analysis of our transgenic FTSH12 lines revealed large changes in the total protein extract, with >45% of all quantified proteins exhibiting significant changes in abundance amongst the three lines. In line with the pale-green phenotype, plastid proteins including proteins associated with photosynthesis, chlorophyll biosynthesis and maintenance of the photosynthetic machinery, were depleted in the mi12-3 line, whereas proteins associated with lytic compartments and catabolic processes accumulated (Supplementary Table S6). In contrast, ox12-1 contained higher amounts of photosynthesis-related proteins compared with wild type, suggesting accelerated plastid development and higher chlorophyll content during de-etiolation (Fig. 2C). Interestingly, the different FtsH12 motor complex subunits showed differential expression in the mutants (Table 2). FtsHi subunits faithfully reflected FtsH12 abundance and accumulated in the overexpressor line ox 12-1, but dropped below detection limits in the knock-down line mi2-3. As expected for a protein with a major metabolic function, pdNAD-MDH was much more abundant than the other subunits and did not show significant differences between wild type and mi12-3, suggesting that only a minor fraction of the total pdNAD-MDH is involved in the moonlighting function in the FtsH12 complex (Schreier et al., 2018). In contrast, YCF2, the only plastid-encoded putative interaction partner of FtsH12, showed a moderately increased abundance in wild type, but no significant difference between ox 12-1 overexpressor and mi12-3 knock-down line. At the transcript level the expression of YCF2 followed the transcription patterns of the well-known TIC import machinery (Supplementary Fig. S9). Also, pull-down experiments of proteins cross-linked to translocating model proteins clearly identified all four FtsHi subunits and YCF2, but only trace amounts of FtsH12 (Kikuchi et al., 2018), while we did not detect YCF2 in our immunoprecipitation experiments with Myc-tagged FtsH12 expressed from its native promoter. Interestingly, FtsH12 was recently also found in a complex with FtsHi1,2,4,5 and plastid pdNAD-MDH using a combination of native gel electrophoresis and absolute protein

quantification by MS (Schäfer et al., 2019). YCF2 was not detected in this study. Although expressed at low absolute levels, FtsH12 appeared twice as abundant as the FtsHi subunits in the complex (Schäfer et al., 2019). One might therefore speculate that accumulation of the FtsH12/FtsHi complex depends on the amount of FtsH12, possibly in a 1:2 stoichiometry of FtsH12 to FtsHi, similar to the ratio of A-type and B-type FtsH proteases in the thylakoid FtsH complex (Kato and Sakamoto, 2018), whereas YCF2 accumulates as a stable protein, independent of FtsH12. However, further experiments are required to determine the stoichiometry of the complex and answer the question as to whether YCF2 is indeed absent from the FtsH12/FtsHi/pdNAD-MDH complex at native expression levels, or if we lost the protein due to the chosen buffer and wash conditions.

Based on the proposed function of the FtsH12 complex as an import motor (Kikuchi et al., 2018), the phenotype of FTSH12 knock-down might limit protein import efficiency via the 1 MDa TIC complex. The accumulation of TIC20/56/100/214 subunits in the knock-down mutant compared with wild type (Table 2) might be explained by a partial compensation of the limited import capacity by an increase in the number of TIC complexes, possibly in conjunction with the association of an alternative motor complex. Although most other identified TIC components showed no significant changes, TIC22-III accumulated in the knock-down mutant compared with wild type. This may further indicate a modified import complex composition to compensate for the lack of FtsH12, as TIC22-III has been suggested to participate in chloroplast protein import when the required import rate is as high as during early development (Rudolf et al., 2013). Unfortunately we were not able to isolate intact chloroplasts from the mi12 knock-down mutants, and therefore could not test this attractive hypothesis with import experiments.

Compared with other active FtsH proteases, FtsH12 contains several amino acid exchanges in the Walker B motif and the second region of homology of its AAA-type domain that likely impair the ATPase activity function. In canonical FtsH proteases, ATPase activity is required for extraction and presentation of membrane protein substrates to the protease domain (Bieniossek et al., 2009). Thus, formation of a complex with the proteolytically inactive FtsHi members may be required to enable proteolytic activity of FtsH. Assuming a degradative function of FtsH12, proteins accumulating in the miRNA mutant compared with wild type and/or the overexpression line (clusters 2 and 5; Fig. 5) that are located in the chloroplast envelope appear as the most likely candidate substrates. However, this cluster included few envelope proteins, and most of these, such as the fatty acid transporter FAX1 and components of the chloroplast import machinery that were reported as general features of albino/pale-green mutants, mitigate the lack of protein import capacity and photosynthesis (Motohashi et al., 2012). Also the increased protein abundance of the TIC components accumulating in mi12-3 appears to arise from transcriptional changes (Supplementary Fig. S9) and not from lack of FtsH12mediated degradation. In addition, a proteolytically inactive FtsH12 variant has been reported to complement an embryolethal T-DNA insertion line, demonstrating that the protease activity was not required for its essential function (Kikuchi et al., 2018). We hypothesized that FtsH12 might affect protein processing either directly by its proteolytic activity or indirectly through impairment of normal proteolytic maturation after import. However, our N-terminome analysis revealed overall good correlation of protein N-termini abundance and protein abundance. The few protein N-termini with strong changes in abundance and unchanged protein abundance were manually inspected, but did not include protease-generated termini of plastid proteins, and therefore, likely represent indirect effects arising from differential activation of other proteolytic activities, as for example lytic enzymes in the vacuole. We further hypothesized that impaired protein import due to lack of FtsH12 might lead to a backlog of unprocessed precursor proteins, and indeed identified 12 N-terminal peptides of nuclear-encoded plastid proteins that mapped to position 2 of the protein model, indicating intact chloroplast targeting peptides (Supplementary Table S7). Eleven of these did not contain a Lys that would allow quantification in our assay, while the remaining precursor of an uncharacterized protein encoded by gene At4g28440 showed no significant difference in accumulation. This was not unexpected, as unprocessed precursor proteins accumulating in the cytosol are rapidly degraded by the ubiquitin/proteasome system (Lee et al., 2009; Grimmer et al., 2020).

In conclusion our data confirm the existence of a heteromeric FtsH12 complex with FtsHi1, FtsHi2, FtsHi4, FtsHi5 and pdNAD-MDH in the inner chloroplast envelope membrane (Kikuchi et al., 2018; Schreier et al., 2018; Schäfer et al., 2019). Plants with modulated expression of FtsH12 showed dramatic changes in proteome composition, and demonstrate that the abundance of FtsH12 regulates the accumulation of the FtsHi subunits, but not pdNAD-MDH or YCF2. Plants with reduced FTSH12 expression were impaired in the formation of thylakoid membranes, whereas FTSH12 overexpressing plants appeared to develop slightly faster. N-terminome profiling demonstrated unaltered maturation of chloroplast-imported proteins, irrespective of the abundance of FtsH12.

Supplementary data

The following supplementary data are available at *JXB* online. Fig. S1. Domain structure of FtsH12.

Fig. S2. Expression of FTSH12 in different organs of A. thaliana (Col-0) and during different developmental stages. Fig. S3. Expression of FtsH12 during development.

Fig. S4. Sub-organellar location of FtsH12 in chloroplasts.

Fig. S5. Identification of homozygous T2 FtsH12-4x-c-myc T-DNA insertion into FTSH12.

Fig. S6. Analysis of co-immunoprecipitation experiments.

Fig. S7. Phenotypic comparison of wild type, FtsH12 overexpressor and knock-down plants.

Fig. S8. Occurrence of reactive oxygen species in wild type and FTSH12 transgenic lines.

Fig. S9. Transcript abundance of import complex subunits.

Fig. S10. Graphical depiction of protein interactions in Cluster 1 of the proteome analysis.

Fig. S11. Graphical depiction of protein interactions in Cluster 2 of the proteome analysis.

Fig. S12. Graphical depiction of protein interactions in Cluster 3 of the proteome analysis.

Fig. S13. Graphical depiction of protein interactions in Cluster 4 of the proteome analysis.

Fig. S14. Graphical depiction of protein interactions in Cluster 5 of the proteome analysis.

Fig. S15. Graphical depiction of protein interactions in Cluster 6 of the proteome analysis.

Fig. S16. Graphical depiction of protein interactions in Cluster 7 of the proteome analysis.

Fig. S17. Quantitative N-terminome analysis in FtsH12 mutants compared with wild type.

Table S1. Sequences of primers used in this study.

Table S2. List of proteins identified my mass spectrometry after FtsH12:Myc immunoprecipitation

Table S3. Densitometric analysis of FtsH12 protein amounts (% of wild type) in 10 day-old ftshi seedlings.

Table S4. Chlorophyll fluorescence parameters.

Table S5. List of 3129 quantified proteins.

Table S6. List of 1450 proteins with significantly changed abundance between mi12-3, ox12-1 and wild type, as determined by ANOVA analysis.

Table S7. List of identified protein N-termini with quantification result and annotation.

Author contributions

KM, RW and LSM were involved in the formal analysis, and generated and characterized the mutant plants; RW, FD and AP performed mass spectrometry experiments; RW, FD, AP and PFH analysed mass spectrometry data; PFH and CF conceived and supervised the project; CF and PFH wrote the manuscript with contributions from all authors; CF conceptualized the project and was responsible for funding acquisition.

Acknowledgements

We acknowledge financial support by the Swedish Research Council VR (grant number 2019-04472 to CF), Umeå University (to CF), the Kempe foundation (to RW), the European Union's Horizon 2020 programme COST action BM1307 "Proteostasis" (STSM grant BM1307 -40169 to RW) and the European Research Council (grant 639905 to PFH). We are grateful for the help by the KBC electron microscopy

platform, supported by Umeå University and the Swedish University of Agricultural Sciences and to Prof. Åsa Strand, Umeå University, for providing us with the Arabidopsis cell line.

Conflict of interest

All authors read and approved the manuscript and have no conflict of interest to disclose.

Data availability

MS data are available on the PRIDE archive (https://www.ebi.ac.uk/ pride/archive/;Vizcaíno et al., 2015; Deutsch et al., 2017) with the accession numbers PXD010619 for proteome, PXD022423 for N-terminome and PXD010615 for AP-MS data. Novel materials described in this paper will be made available for non-commercial research purposes.

References

Adam Z, Aviv-Sharon E, Keren-Paz A, Naveh L, Rozenberg M, Savidor A, Chen J. 2019. The chloroplast envelope protease FTSH11 interaction with CPN60 and identification of potential substrates. Frontiers in Plant Science 10, 428.

Agne B, Köhler D, Baginsky S. 2017. Protein import-independent functions of Tic56, a component of the 1-MDa translocase at the inner chloroplast envelope membrane. Plant Signaling & Behavior 12, e1284726.

Almagro Armenteros JJ, Salvatore M, Emanuelsson O, Winther O, von Heijne G, Elofsson A, Nielsen H. 2019. Detecting sequence signals in targeting peptides using deep learning. Life Science Alliance 2, e201900429

Beck S, Michalski A, Raether O, et al. 2015. The impact II, a very highresolution quadrupole time-of-flight instrument (QTOF) for deep shotgun proteomics. Molecular & Cellular Proteomics 14, 2014-2029.

Benjamini Y, Hochberg Y. 1995. Controlling the false discovery rate: a practical and powerful approach to multiple testing. Journal of the Royal Statistical Society. Series B (Methodological) 57, 289-300.

Bieniossek C, Niederhauser B, Baumann UM. 2009. The crystal structure of apo-FtsH reveals domain movements necessary for substrate unfolding and translocation. Proceedings of the National Academy of Sciences, USA 106, 21579-21584.

Bölter B, Soll J. 2017. Ycf1/Tic214 is not essential for the accumulation of plastid proteins. Molecular Plant 10, 219-221.

Chen L, Shan Y, Weng Y, Sui Z, Zhang X, Liang Z, Zhang L, Zhang Y. 2016. Hydrophobic tagging-assisted N-termini enrichment for in-depth N-terminome analysis. Analytical Chemistry 88, 8390-8395.

Clough SJ, Bent AF. 1998. Floral dip: a simplified method for Agrobacterium-mediated transformation of Arabidopsis thaliana. The Plant Journal 16, 735-743.

Demir F, Niedermaier S, Kizhakkedathu JN, Huesgen PF. 2017. Profiling of protein N-termini and their modifications in complex samples. In: Schilling O, ed. Protein terminal profiling: methods and protocols. New York, NY: Springer New York, 35-50.

Demir F, Niedermaier S, Villamor JG, Huesgen PF. 2018. Quantitative proteomics in plant protease substrate identification. New Phytologist 218, 936-943

Deutsch EW, Csordas A, Sun Z, et al. 2017. The ProteomeXchange consortium in 2017: supporting the cultural change in proteomics public data deposition. Nucleic Acids Research 45, D1100-D1106.

Dubreuil C, Jin X, Barajas-López JD, et al. 2018. Establishment of photosynthesis through chloroplast development is controlled by two distinct regulatory phases. Plant Physiology 176, 1199-1214.

- **Ferro M, Brugière S, Salvi D, et al.** 2010. AT_CHLORO, a comprehensive chloroplast proteome database with subplastidial localization and curated information on envelope proteins. Molecular & Cellular Proteomics **9**, 1063–1084
- Fryer MJ, Oxborough K, Mullineaux PM, Baker NR. 2002. Imaging of photo-oxidative stress responses in leaves. Journal of Experimental Botany 53, 1249–1254.
- Gomez-Auli A, Hillebrand LE, Biniossek ML, Peters C, Reinheckel T, Schilling O. 2016. Impact of cathepsin B on the interstitial fluid proteome of murine breast cancers. Biochimie 122, 88–98.
- **Grimmer J, Helm S, Dobritzsch D, Hause G, Shema G, Zahedi RP, Baginsky S.** 2020. Mild proteasomal stress improves photosynthetic performance in *Arabidopsis* chloroplasts. Nature Communications **11**, 1662.
- **Hartl M, Füßl M, Boersema PJ, et al.** 2017. Lysine acetylome profiling uncovers novel histone deacetylase substrate proteins in *Arabidopsis*. Molecular Systems Biology **13**, 949.
- **Haselmann H, Mannara F, Werner C, et al.** 2018. Human autoantibodies against the AMPA receptor subunit GluA2 induce receptor reorganization and memory dysfunction. Neuron **100**, 91–105.e9.
- **Hellens R, Mullineaux P, Klee H.** 2000. Technical focus:a guide to *Agrobacterium* binary Ti vectors. Trends in Plant Science **5**, 446–451.
- Hofsetz E, Demir F, Szczepanowska K, Kukat A, Kizhakkedathu JN, Trifunovic A, Huesgen PF. 2020. The mouse heart mitochondria N terminome provides insights into ClpXP-mediated proteolysis. Molecular & Cellular Proteomics 19, 1330–1345.
- **Kadirjan-Kalbach DK, Yoder DW, Ruckle ME, Larkin RM, Osteryoung KW.** 2012. *FtsHi1/ARC1* is an essential gene in *Arabidopsis* that links chloroplast biogenesis and division. The Plant Journal **72**, 856–867.
- **Kato Y, Sakamoto W.** 2018. FtsH protease in the thylakoid membrane: physiological functions and the regulation of protease activity. Frontiers in Plant Science **9**, 855.
- **Kikuchi S, Asakura Y, Imai M, et al.** 2018. A Ycf2-FtsHi heteromeric AAA-ATPase complex is required for chloroplast protein import. The Plant Cell **30**, 2677–2703.
- Kikuchi S, Bédard J, Hirano M, Hirabayashi Y, Oishi M, Imai M, Takase M, Ide T, Nakai M. 2013. Uncovering the protein translocon at the chloroplast inner envelope membrane. Science 339, 571–574.
- Kleinboelting N, Huep G, Kloetgen A, Viehoever P, Weisshaar B. 2012. GABI-Kat SimpleSearch: new features of the *Arabidopsis thaliana* T-DNA mutant database. Nucleic Acids Research **40**, D1211–D1215.
- **Knopf RR, Feder A, Mayer K, Lin A, Rozenberg M, Schaller A, Adam Z.** 2012. Rhomboid proteins in the chloroplast envelope affect the level of allene oxide synthase in *Arabidopsis thaliana*. The Plant Journal **72**, 559–571.
- **Kubo M, Udagawa M, Nishikubo N, Horiguchi G, Yamaguchi M, Ito J, Mimura T, Fukuda H, Demura T.** 2005. Transcription switches for protoxylem and metaxylem vessel formation. Genes & Development **19**, 1855–1860.
- **Laemmli UK.** 1970. Cleavage of structural proteins during the assembly of the head of bacteriophage T4. Nature **227**, 680–685.
- Lee S, Lee DW, Lee Y, Mayer U, Stierhof YD, Lee S, Jürgens G, Hwang I. 2009. Heat shock protein cognate 70-4 and an E3 ubiquitin ligase, CHIP, mediate plastid-destined precursor degradation through the ubiquitin-26S proteasome system in *Arabidopsis*. The Plant Cell **21**, 3984–4001.
- **Li Y, Martin JR, Aldama GA, Fernandez DE, Cline K.** 2017. Identification of putative substrates of SEC2, a chloroplast inner envelope translocase. Plant Physiology **173**, 2121–2137.
- **Li HM, Schnell D, Theg SM.** 2020. Protein import motors in chloroplasts: on the role of chaperones. The Plant Cell **32**, 536–542.
- Lu X, Zhang D, Li S, Su Y, Liang Q, Meng H, Shen S, Fan Y, Liu C, Zhang C. 2014. FtsHi4 is essential for embryogenesis due to its influence on chloroplast development in *Arabidopsis*. PLoS One **9**, e99741.
- McAndrew RS, Froehlich JE, Vitha S, Stokes KD, Osteryoung KW. 2001. Colocalization of plastid division proteins in the chloroplast stromal

- compartment establishes a new functional relationship between FtsZ1 and FtsZ2 in higher plants. Plant Physiology **127**, 1656–1666.
- **Meinke D, Muralla R, Sweeney C, Dickerman A.** 2008. Identifying essential genes in *Arabidopsis thaliana*. Trends in Plant Science **13**, 483–491.
- **Mishra LS, Mielke K, Wagner R, Funk C.** 2019. Reduced expression of the proteolytically inactive FtsH members has impacts on the Darwinian fitness of *Arabidopsis thaliana*. Journal of Experimental Botany **70**, 2173–2184.
- **Motohashi R, Rödiger A, Agne B, Baerenfaller K, Baginsky S.** 2012. Common and specific protein accumulation patterns in different albino/pale-green mutants reveals regulon organization at the proteome level. Plant Physiology **160**, 2189–2201.
- **Murashige T, Skoog F.** 1962. A revised medium for rapid growth and bio assays with tobacco tissue cultures. Physiologia Plantarum **15**, 473–497.
- **Nakai M.** 2015. The TIC complex uncovered: the alternative view on the molecular mechanism of protein translocation across the inner envelope membrane of chloroplasts. Biochimica et Biophysica Acta **1847**, 957–967.
- **Nakai M.** 2018. New perspectives on chloroplast protein import. Plant & Cell Physiology **59**, 1111–1119.
- **Nakai M.** 2020. Reply: the revised model for chloroplast protein import. The Plant Cell **32**, 543–546.
- Nakata M, Mitsuda N, Herde M, Koo AJ, Moreno JE, Suzuki K, Howe GA, Ohme-Takagi M. 2013. A bHLH-type transcription factor, ABA-INDUCIBLE BHLH-TYPE TRANSCRIPTION FACTOR/JA-ASSOCIATED MYC2-LIKE1, acts as a repressor to negatively regulate jasmonate signaling in *Arabidopsis*. The Plant Cell **25**, 1641–1656.
- **Okuno T, Ogura T.** 2013. FtsH protease-mediated regulation of various cellular functions. Sub-cellular Biochemistry **66**, 53–69.
- **Perrar A, Dissmeyer N, Huesgen PF.** 2019. New beginnings and new ends: methods for large-scale characterization of protein termini and their use in plant biology. Journal of Experimental Botany **70**, 2021–2038.
- **Pesquet E, Korolev AV, Calder G, Lloyd CW.** 2010. The microtubule-associated protein AtMAP70-5 regulates secondary wall patterning in *Arabidopsis* wood cells. Current Biology **20**, 744–749.
- **Porra RJ, Thompson WA, Kriedemann PE.** 1989. Determination of accurate extinction coefficients and simultaneous equations for assaying chlorophylls *a* and *b* extracted with four different solvents: verification of the concentration of chlorophyll standards by atomic absorption spectroscopy. Biochimica et Biophysica Acta (BBA) Bioenergetics **975**, 384–394.
- **Putarjunan A, Liu X, Nolan T, Yu F, Rodermel S.** 2013. Understanding chloroplast biogenesis using second-site suppressors of *immutans* and *var2*. Photosynthesis Research **116**, 437–453.
- **Rappsilber J, Mann M, Ishihama Y.** 2007. Protocol for micro-purification, enrichment, pre-fractionation and storage of peptides for proteomics using StageTips. Nature Protocols **2**, 1896–1906.
- **Rawlings ND, Barrett AJ, Thomas PD, Huang X, Bateman A, Finn RD.** 2017. The *MEROPS* database of proteolytic enzymes, their substrates and inhibitors in 2017 and a comparison with peptidases in the PANTHER database. Nucleic Acids Research **46**, D624–D632.
- Ritchie ME, Diyagama D, Neilson J, van Laar R, Dobrovic A, Holloway A, Smyth GK. 2006. Empirical array quality weights in the analysis of microarray data. BMC Bioinformatics 7, 261.
- **Rowland E, Kim J, Bhuiyan NH, van Wijk KJ.** 2015. The *Arabidopsis* chloroplast stromal N-terminome: complexities of amino-terminal protein maturation and stability. Plant Physiology **169**, 1881–1896.
- **Rudolf M, Machettira AB, Groß LE, et al.** 2013. *In vivo* function of Tic22, a protein import component of the intermembrane space of chloroplasts. Molecular Plant **6**, 817–829.
- **Salvesen GS, Hempel A, Coll NS.** 2016. Protease signaling in animal and plant-regulated cell death. The FEBS Journal **283**, 2577–2598.
- Schäfer P, Helm S, Köhler D, Agne B, Baginsky S. 2019. Consequences of impaired 1-MDa TIC complex assembly for the abundance and composition of chloroplast high-molecular mass protein complexes. PLoS One 14, e0213364.

Schreier TB, Cléry A, Schläfli M, et al. 2018. Plastidial NAD-dependent malate dehydrogenase: a moonlighting protein involved in early chloroplast development through its interaction with an FtsH12-FtsHi protease complex. The Plant Cell 30, 1745-1769.

Schwab R, Ossowski S, Riester M, Warthmann N, Weigel D. 2006. Highly specific gene silencing by artificial microRNAs in Arabidopsis. The Plant Cell 18, 1121-1133.

Sedaghatmehr M, Mueller-Roeber B, Balazadeh S. 2016. The plastid metalloprotease FtsH6 and small heat shock protein HSP21 jointly regulate thermomemory in Arabidopsis. Nature Communications 7, 12439.

Sun X. Feng P. Xu X. Guo H. Ma J. Chi W. Lin R. Lu C. Zhang L. 2011. A chloroplast envelope-bound PHD transcription factor mediates chloroplast signals to the nucleus. Nature Communications 2. 477.

Szklarczyk D, Gable AL, Lyon D, et al. 2018. STRING v11: proteinprotein association networks with increased coverage, supporting functional discovery in genome-wide experimental datasets. Nucleic Acids Research 47, D607-D613.

Towbin H. Staehelin T. Gordon J. 1979. Electrophoretic transfer of proteins from polyacrylamide gels to nitrocellulose sheets: procedure and some applications. Proceedings of the National Academy of Sciences, USA 76, 4350-4354.

Turk B, Turk D, Turk V. 2012. Protease signalling: the cutting edge. The EMBO Journal 31, 1630-1643.

Tvanova S, Temu T, Cox J. 2016a. The MaxQuant computational platform for mass spectrometry-based shotgun proteomics. Nature Protocols 11, 2301-2319

Tyanova S, Temu T, Sinitcyn P, Carlson A, Hein MY, Geiger T, Mann M, Cox J. 2016b. The Perseus computational platform for comprehensive analysis of (prote)omics data. Nature Methods 13, 731-740.

Vielle-Calzada JP, Baskar R, Grossniklaus U. 2000. Delayed activation of the paternal genome during seed development, Nature 404, 91–94.

Vizcaíno JA, Csordas A, del-Toro N, et al. 2015. 2016 update of the PRIDE database and its related tools. Nucleic Acids Research 44, D447-D456.

Wagner R, Aigner H, Funk C. 2012. FtsH proteases located in the plant chloroplast. Physiologia Plantarum 145, 203-214.

Wagner R, Aigner H, Pružinská A, Jänkänpää HJ, Jansson S, Funk C. 2011. Fitness analyses of Arabidopsis thaliana mutants depleted of FtsH metalloproteases and characterization of three FtsH6 deletion mutants exposed to high light stress, senescence and chilling. New Phytologist 191, 449-458.

Wagner R, von Sydow L, Aigner H, Netotea S, Brugière S, Sjögren L, Ferro M, Clarke A, Funk C. 2016. Deletion of FtsH11 protease has impact on chloroplast structure and function in Arabidopsis thaliana when grown under continuous light. Plant, Cell & Environment **39**. 2530-2544.

Wang T, Li S, Chen D, Xi Y, Xu X, Ye N, Zhang J, Peng X, Zhu G. 2018. Impairment of FtsHi5 function affects cellular redox balance and photorespiratory metabolism in Arabidopsis. Plant & Cell Physiology 59, 2526-2535

Weng SSH, Demir F, Ergin EK, Dirnberger S, Uzozie A, Tuscher D, Nierves L, Tsui J, Huesgen PF, Lange PF. 2019. Sensitive determination of proteolytic proteoforms in limited microscale proteome samples. Molecular & Cellular Proteomics 18, 2335-2347.

Wessel D, Flügge UI. 1984. A method for the quantitative recovery of protein in dilute solution in the presence of detergents and lipids. Analytical Biochemistry 138, 141-143.